

Review

Optoelectronic Oscillators: Progress from Classical Designs to Integrated Systems

Qidi Liu ¹, Jiuchang Peng ² and Juanjuan Yan ^{2,*}

¹ School of Electrical and Computer Engineering, University of Georgia, Athens, GA 30602, USA; qidi.liu.photonics@gmail.com

² School of Electronic Information Engineering, Beihang University, Beijing 100191, China; pengjiuchang@buaa.edu.cn

* Correspondence: yanjuanjuan@buaa.edu.cn

Abstract: Optoelectronic oscillators (OEOs) have emerged as indispensable tools for generating low-phase-noise microwave and millimeter-wave signals, which are critical for a variety of high-performance applications. These include radar systems, satellite links, electronic warfare, and advanced instrumentation. The ability of OEOs to produce signals with exceptionally low phase noise makes them ideal for scenarios demanding high signal purity and stability. In radar systems, low-phase-noise signals enhance target detection accuracy and resolution, while, in communication networks, such signals enable higher data throughput and improved signal integrity over extended distances. Furthermore, OEOs play a pivotal role in precision instrumentation, where even minor noise can compromise the performance of sensitive equipment. This review examines the progress in OEO technology, transitioning from classical designs relying on long optical fiber delay lines to modern integrated systems that leverage photonic integration for compact, efficient, and tunable solutions. Key advancements, including classical setups, hybrid designs, and integrated configurations, are discussed, with a focus on their performance improvements in phase noise, side-mode suppression ratio (SMSR), and frequency tunability. A 20-GHz oscillation with an SMSR as high as 70 dB has been achieved using a classical dual-loop configuration. A 9.867-GHz frequency with a phase noise of -142.5 dBc/Hz @ 10 kHz offset has also been generated in a parity-time-symmetric OEO. Additionally, integrated OEOs based on silicon photonic microring resonators have achieved an ultra-wideband tunable frequency from 3 GHz to 42.5 GHz, with phase noise as low as -93 dBc/Hz at a 10 kHz offset. The challenges in achieving fully integrated OEOs, particularly concerning the stability and phase noise at higher frequencies, are also explored. This paper provides a comprehensive overview of the state of the art in OEO technology, highlighting future directions and potential applications.

Received: 19 December 2024

Revised: 18 January 2025

Accepted: 26 January 2025

Published: 29 January 2025

Citation: Liu, Q.; Peng, J.; Yan, J.

Optoelectronic Oscillators: Progress from Classical Designs to Integrated Systems. *Photonics* **2025**, *12*, 120.

[https://doi.org/10.3390/](https://doi.org/10.3390/photronics12020120)

[photronics12020120](https://doi.org/10.3390/photronics12020120)

Copyright: © 2025 by the authors.

Submitted for possible open access publication under the terms and conditions of the Creative Commons Attribution (CC BY) license (<https://creativecommons.org/licenses/by/4.0/>).

Keywords: OEO; microwave photonics; optical signal processing; integrated photonics

1. Introduction

Optoelectronic oscillators (OEOs) have emerged as an indispensable technology in microwave photonics due to their ability to generate microwave signals with ultra-low-phase noise and a broad bandwidth. OEOs have been extensively utilized in high-performance applications such as radar systems, communications, and signal processing. By incorporating optical components such as modulators and photodetectors, OEOs

overcome the limitations of traditional microwave oscillators, significantly improving the phase noise performance and spectral purity [1]. The hybrid nature of OEOs, which combines optical and electronic feedback loops, allows them to generate high-frequency microwave signals, making them ideal for applications that demand precise and stable signal generation.

The development of OEOs began in the late 1990s, following the seminal work of Yao and Maleki, who introduced a fiber-based OEO architecture. This design utilized a long, low-loss optical fiber as an energy storage element, achieving a high-quality factor and reducing the phase noise [2]. This foundational work led to various advancements in OEO architectures, including dual-loop OEOs [3], coupled OEOs (COEOs) [4], and high-Q resonator-based OEOs [5]. These innovations have not only improved the phase noise performance but have also enhanced the flexibility and tunability of OEO systems, thus broadening their applications in modern technology.

One of the most attractive features of OEOs is their ability to generate ultra-low-phase noise signals, which are crucial in applications like radar and communication systems that require short-term frequency stability [6]. Traditional electronic oscillators, such as phase-locked loops (PLLs), dielectric resonator oscillators (DROs), and voltage-controlled oscillators (VCOs), have achieved significant progress in generating stable, high-frequency microwave signals, especially with advancements in semiconductor technologies. However, as frequencies approach the millimeter-wave range, electronic oscillators often face increased phase noise, limited frequency tunability, electromagnetic interference (EMI), and signal integrity challenges due to parasitic effects and thermal noise. Therefore, traditional electronic oscillators struggle to maintain signal quality as the frequency increases, but OEOs leverage the advantages of photonics to achieve stable, high-frequency microwave signals, making them another alternative for these high-performance applications [7]. The integration of optical delay lines or high-quality resonators in the OEO feedback loop has been key to achieving this low phase noise, as these components provide the high-quality factor necessary for noise reduction [8].

In recent years, there has been growing interest in integrated OEOs, which aims to miniaturize the technology while maintaining the excellent performance. Photonic integration platforms [9–11], such as silicon and indium phosphide, have enabled the fabrication of compact OEOs with a low power consumption, which are critical for next-generation communication systems and sensors [12]. Additionally, techniques for mode control and frequency tunability, such as the use of tunable microwave photonic filters [13] and optoelectronic parametric processes [14,15], have expanded the versatility of OEOs in producing a variety of microwave signals, including chirped and complex waveforms.

While several reviews have discussed OEOs, most focus narrowly on either classical designs or specific performance aspects without fully exploring the progression to integrated systems. For example, [16] offers a comprehensive overview of traditional OEO structures, primarily emphasizing frequency stability enhancement and phase noise reduction techniques, while [17,18] focus on the integration of OEOs in microwave photonic systems. In contrast, our review offers a comprehensive analysis of OEO technology, tracing its evolution from classical discrete-component architectures to advanced integrated systems. We uniquely highlight the role of emerging materials and innovative designs, such as parity–time (PT)-symmetric and hybrid OEOs. Additionally, we provide comparative evaluations of different integration platforms and up-to-date insights into broadband and frequency-tunable OEOs, incorporating the latest developments from 2023 and 2024. This holistic perspective not only captures the current state of the field but also identifies challenges and opportunities for future research in OEO technology.

This review explores the evolution of OEOs, focusing on their transition from traditional fiber-based architectures to advanced integrated systems. We discuss the

fundamental principles that support their operation, analyze key technological advancements in designs such as hybrid integration, parity–time-symmetric systems, and microring resonator-based configurations, and examine their performance improvements in terms of phase noise, frequency tunability, and compactness. By presenting a comprehensive overview of these developments, this review highlights the current state of OEO technology and its growing potential for applications in fields such as radar, wireless communications, and precision instrumentation, while addressing the challenges that remain for achieving high-performance, fully integrated systems.

2. OEO Configurations and Architectures

2.1. Single-Loop OEOs

A typical single-loop OEO is depicted schematically in Figure 1. The optical carrier generated by a laser diode (LD) is intensity-modulated by the feedback signal using an electro-optic modulator (EOM). This modulator can be either a Mach–Zehnder modulator (MZM) [4,19,20] or an electroabsorption modulator (EAM), the latter offering the advantages of a low driving voltage and high integration capability [21,22]. The modulated optical signal, after amplification by an optical amplifier (OA), propagates through a length of single-mode fiber (SMF) and is subsequently converted into an electrical signal by a photodetector (PD). The electrical signal is then amplified by an electrical amplifier (EA), and an electrical bandpass filter (EBPF) is employed to perform the mode selection. The filtered signal is divided into two parts by an electrical coupler (EC). One part is adjusted via a phase shifter (PS) and fed back to the EOM, thereby establishing a closed positive feedback loop. Another part is output or observed with an electrical signal analyzer (ESA).

When a MZM is used and the driving signal applied to the modulator is $V_{in}(t)$, the output of the MZM is

$$E_{out}(t) = E_{in}(t) \cos \left[\frac{\pi V_{in}(t)}{V_{\pi}} + \frac{\varphi}{2} \right] e^{j\frac{\varphi}{2}} \quad (1)$$

where $E_{in}(t)$ is the optical carrier from the LD, $\varphi = \pi V_b/V_{\pi}$ is the phase shift induced by the DC bias voltage V_b , and V_{π} is the half-wave voltage of the MZM. After transmission through the OEO loop, the output signal of the PS $V_{out}(t)$ can be obtained as

$$V_{out}(t) = \frac{1}{2} R R_d \gamma G_e G_o P_o e^{-\alpha L} \cos \left[\frac{2\pi V_{in}(t)}{V_{\pi}} + \varphi \right] \quad (2)$$

where R is the responsivity of the PD, R_d is the load impedance of the photodetector, γ is the amplitude attenuation due to the EBPF, EC and PS, G_e is the voltage gain of the EA, G_o is the gain of the OA, P_o is the average output power of the LD, and α and L are, respectively, the attenuation coefficient and length of the fiber.

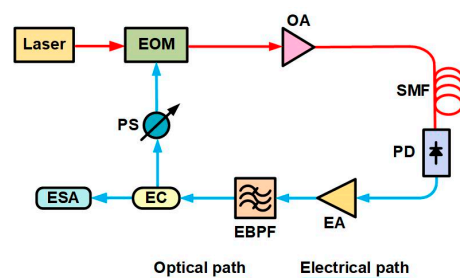


Figure 1. Schematic diagram of a typical single-loop OEO.

Then, the small-signal open-loop gain of the OEO is

$$G_s = \left. \frac{dV_{out}}{dV_{in}} \right|_{V_{in}=0} = -\frac{\pi RR_d \gamma G_e G_o P_o e^{-\alpha L} \sin \varphi}{V_\pi} \quad (3)$$

To achieve a stable oscillation in an OEO, optical and electrical amplifiers are used to provide sufficient gain to make the net gain $|G_s|$ greater than 1. Additionally, the phase-matching condition to be satisfied is [1]

$$\omega_k \tau + \phi(\omega_k) + \phi_0 = 2k\pi, \quad k = 0, 1, 2, \dots \quad (4)$$

Here, k represents the mode number, ω_k denotes the angular frequency of the k -th mode, τ is the time delay determined by the physical length of the feedback loop, $\phi(\omega_k)$ is the frequency-dependent phase induced by the dispersive components in the loop, and ϕ_0 is the initial phase. Theoretical analysis has suggested that modes satisfying the gain and phase-matching conditions can initiate oscillation. The frequency spacing between two adjacent oscillation modes, known as the Free Spectral Range (FSR), is inversely proportional to the loop delay. Typically, an EBPF is employed to select oscillation modes. Within the EBPF's passband, the strongest primary mode, located near the center frequency, may coexist with weaker side modes if the FSR is smaller than the filter bandwidth. However, due to the saturation of the gain medium and the nonlinear behavior of the EOM, the gains of oscillating modes gradually converge to unity. As a result, only the mode closest to the EBPF's center frequency survives, forming a stable oscillation.

2.2. Performance Parameters

The critical performance parameters of OEOs include the side-mode suppression ratio (SMSR) and phase noise, which are directly related to the spectral purity and stability of the generated oscillating signal, respectively. Additionally, power consumption is an important factor for the practical deployment of OEOs. Traditional, unintegrated OEOs typically consume more power than conventional microwave oscillators due to the additional energy required to drive the optical modulator and support fiber-based optical amplification. However, OEOs offer significant advantages, including a wider operational bandwidth, higher spectral purity, and lower phase noise. Moreover, with the advancement of photonic integration, the overall power consumption of OEOs can be significantly reduced, enhancing their practicality for real-world applications.

2.2.1. Side-Mode Suppression Ratio

The SMSR parameter quantifies the spectral purity of the oscillating signal output from an OEO. It is defined as

$$SMSR = 10 \lg \left(\frac{P_{main}}{P_{side}} \right) \quad (5)$$

where P_{main} is the power of the main oscillation mode and P_{side} is the maximum power of the side modes. A higher SMSR indicates superior spectral purity, which is essential for applications requiring clean and stable signals.

As discussed earlier, the single-frequency mode in OEOs is typically selected using an EBPF. However, in long fiber loops, the small FSR results in a higher density of side modes within the EBPF passband, which degrades the SMSR. To address this issue, one common approach involves employing a multi-loop structure, which increases the effective FSR through gain competition among multiple sets of modes [23]. Another effective strategy to suppress side modes and achieve single-frequency oscillation is replacing long optical fibers with high-Q optical resonators as the optical energy storage medium, where the Q-factor is defined as

$$Q = 2\pi f_{osc} \tau \quad (6)$$

where f_{osc} is the oscillation frequency and τ is the loop delay; the Q-factor is defined as $Q = 2\pi f_{osc}\tau$ and f_{osc} is the oscillation frequency. High-Q optical resonators, such as microring resonators (MRRs), significantly improve the spectral purity due to their large FSRs and high Q-factors [5].

2.2.2. Phase Noise

The phase noise of an oscillator is defined as the ratio of the noise power in a 1 Hz bandwidth at a certain offset frequency to the signal power at the central frequency. It is measured in dBc/Hz and characterized as the single-sideband (SSB) phase noise. According to Leeson model, the output phase noise power spectral density of an OEO can be expressed as [24]

$$S_{\phi_o}(f) = S_{\phi_i}(f) \left[1 + \left(\frac{f_{osc}}{2fQ} \right)^2 \right] \quad (7)$$

where $S_{\phi_i}(f)$ is the input phase noise power spectral density and f is the frequency offset from the oscillation frequency. The input phase noise in OEOs includes the relative intensity noise (RIN), shot noise, thermal noise, and flicker noise. The RIN originates from the laser, whose intensity fluctuations are converted into current fluctuations by the photodetector. Shot noise is mainly caused by the statistical fluctuations of carriers within the OEOs. Thermal noise primarily originates from RF amplifiers and PDs, resulting from the random motion of electrons excited by heat. Flicker noise is a low-frequency noise source from RF amplifiers and PD, impacting the phase noise near the oscillation frequency. The total input phase noise power spectral density S_{ϕ_i} can be expressed as

$$S_{\phi_i} = \frac{N_{RIN} I_{ph}^2 R_d + 2e I_{ph} R_d + 2k_B T_e N_F}{P_{osc}} + b_{-1}/f \quad (8)$$

where N_{RIN} is the RIN noise of the laser, I_{ph} is the photocurrent, e is the electron charge, k_B is the Boltzmann constant, T_e is the room temperature, N_F is the noise figure of the EA, b_{-1} is the total flicker noise coefficient of the EA and PD, and P_{osc} is the oscillation power before the EA.

2.3. Dual-Loop OEOs

According to Equations (6) and (7), in single-loop OEOs, a long optical fiber with a low transmission loss is commonly employed to construct a resonant cavity with a high Q-factor, enabling the generation of low-phase-noise signals. However, the use of long fibers introduces a small FSR, which complicates the mode selection and can lead to issues such as mode hopping and a degraded SMSR. To address these challenges, dual-loop OEOs have been proposed [23,25], where two loops with different length are incorporated.

As illustrated in Figure 2, in a typical dual-loop OEO configuration, the modulated optical signal is amplified and divided by an optical coupler into two paths, each feeding a long and a short optical fiber loop. These signals are converted into electrical signals by two PDs and then combined by an EC. In this configuration, an EA and a PS are also used to satisfy the gain and the phase conditions for oscillating, and an EBPF is for mode selection. The long optical loop forms a high-Q resonant cavity, reducing the phase noise of the output signal, while the short loop assists in mode selection, thereby improving the SMSR. By designing the fiber lengths of the loops in a multiple relationship, the system allows for different oscillation modes to form in each loop. Only the common modes in the two loops are output. In this case, the oscillation frequency can be expressed as

$$f = m \times FSR_1 = n \times FSR_2 \quad (9)$$

where m and n are integers, and FSR_1 and FSR_2 are the FSRs of the long and short fiber loops, respectively. Due to the Vernier effect, the equivalent mode spacing of the dual-loop OEO is significantly increased, optimizing the SMSR while maintaining the low phase noise.

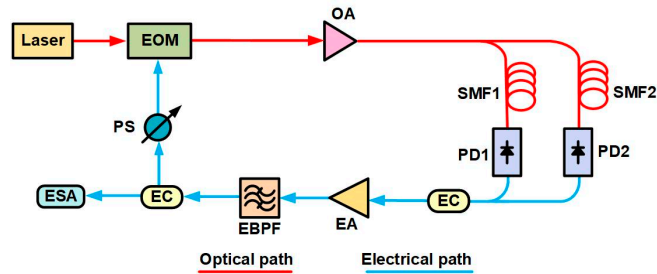


Figure 2. Schematic diagram of a typical dual-loop OEO.

In a dual-loop OEO, optical coupling technology can be used as an alternative to electrical coupling. In the optical domain, polarization division multiplexing enables the use of a polarization beam splitter (PBS) to divide the modulated optical signal into two loops, which are later recombined in the optical domain with a polarization beam combiner (PBC) [26,27]. This approach eliminates the need for multiple independent PDs, thus simplifying the system architecture.

Additionally, dual-loop OEOs can incorporate multiple laser sources by leveraging wavelength division multiplexing (WDM) technology. Wavelength division multiplexers are used in the optical domain to split and combine signals based on their wavelengths. Compared to polarization-based methods, WDM-based systems offer the advantage of reduced interference between beams of different wavelengths, as opposed to the orthogonal polarizations in PBS or PBC configurations. This significantly mitigates the beating noise caused by random interference, enhancing the signal quality and stability [28].

2.4. Coupled OEOs

Both single-loop and dual-loop OEOs utilize long optical fibers to achieve a high Q-factor, which is essential for reducing the phase noise. However, increasing the length of the optical fiber also amplifies its dispersion and sensitivity to environmental perturbations, which can negatively impact the stability of the OEOs. To address these issues and maintain a high Q-factor with shorter optical fibers, the coupled optoelectronic oscillator (COEO), also known as a regenerative mode-locked laser, has been investigated [29,30].

A typical COEO configuration is shown in Figure 3, consisting of the following two coupled loops: a mode-locked laser loop and an OEO loop. The mode-locked laser loop is formed by an optical coupler (OC), an OA, an optical filter (OF), a polarization controller (PC), and an MZM. The OEO loop includes a PD, an EBPF, an EA, a PS, and a shared MZM. Unlike traditional OEOs, COEOs do not require external light sources, as the optical signal is generated within the mode-locked laser loop.

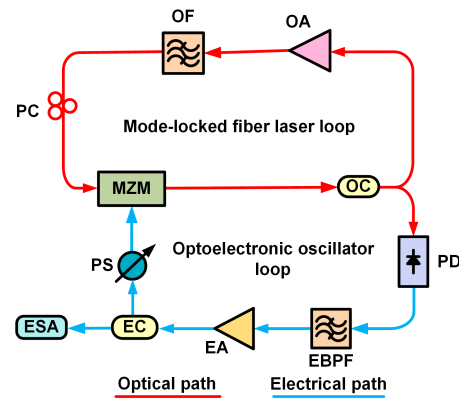


Figure 3. The typical structure of a COEO.

In COEOs, one part of the optical signal produced by the mode-locked laser loop serves as the light source for the OEO loop. After photoelectric conversion, filtering, and amplification, the signal is fed back to the MZM to modulate the gain of the mode-locked laser loop. When the modulation frequency, determined by center of the EBPf, matches an integer multiple of the FSR of the laser loop, mode locking occurs. This ensures that only a subset of the laser modes oscillate in phase, with the mode spacing corresponding to the oscillation frequency of the OEO loop. These selected laser modes are injected into the OEO loop, amplifying the desired oscillation mode while suppressing the others. After multiple iterations, the COEO reaches a stable state, producing a microwave signal with low phase noise and simultaneously outputting an optical pulse with low timing jitter.

The integration of the mode-locked laser loop in the COEO architecture significantly enhances the equivalent Q-factor, reducing the phase noise of the output signal for a given optoelectronic loop delay. This reduces the system’s dependency on long optical fibers, increasing the FSR and relaxing the performance requirements of the EBPf. Consequently, COEOs achieve an improved SMSR and overall system stability while maintaining compactness and efficiency.

2.5. Parity–Time-Symmetric OEOs

Recently, the parity–time (PT)-symmetric OEO has emerged as a novel approach to achieving single-frequency oscillation without relying on narrowband EBPfs. Compared to conventional methods, PT-symmetric OEOs generate high-spectral-purity signals even with small FSRs. A typical PT-symmetric OEO consists of the following two coupled loops of identical lengths: one providing gain and the other providing loss. The PT-symmetry condition requires the gain and loss to be balanced in magnitude. By manipulating the gain, loss, and coupling ratio between the loops, PT-symmetry can be selectively broken for a specific mode, allowing it to dominate and achieve stable single-mode oscillation.

The oscillation mode is governed by a set of coupled differential equations that describe the amplitudes of the *n*th longitudinal mode $a_n^{(1,2)}$ in each loop [31], as follows:

$$\frac{da_n^{(1)}}{dt} = (j\Delta\omega_n^{(1)} + g)a_n^{(1)} - \mu a_n^{(2)} \tag{10}$$

$$\frac{da_n^{(2)}}{dt} = (j\Delta\omega_n^{(2)} - \gamma)a_n^{(2)} - \mu a_n^{(1)} \tag{11}$$

where g and γ represent the net gain or loss in the responding loop, μ is the coupling coefficient between the two loops, ω_n is the angular frequency of the *n*th mode, $\omega_n^{(1,2)}$ are the resonance frequencies of each loop, and $\Delta\omega_n^{(1,2)} = \omega_n - \omega_n^{(1,2)}$ are the detuned frequencies

of each loop. The solution to these equations provides the eigenfrequencies of the system, enabling the identification of the stable oscillation mode when PT symmetry is broken.

PT-symmetric OEOs often adopt a dual-loop structure, where the gain and loss in each loop are controlled via amplifiers and attenuators [31] or with polarization-based methods [32,33]. In addition, a single-loop PT-symmetric OEO based on WDM has been proposed. In this design, the gain, loss, and coupling ratio of equivalent loops are adjusted by tuning the input wavelength based on the reflection characteristics of a chirped fiber Bragg grating (CFBG) [34].

In a PT-symmetric dual-loop OEO configuration, as shown in Figure 4a [31], a stable single-mode oscillation can be achieved with ultralow phase noise. For example, a single-frequency signal at 4.0703 GHz exhibited a phase noise of -108 dBc/Hz at a 10 kHz offset when the loop length was 54.75 m. When a longer loop length of 3216 m was employed, an ultralow phase noise of -139 dBc/Hz at a 10 kHz offset was achieved. These results demonstrate the potential of PT-symmetric OEOs for producing high-spectral-purity signals while maintaining a low phase noise.

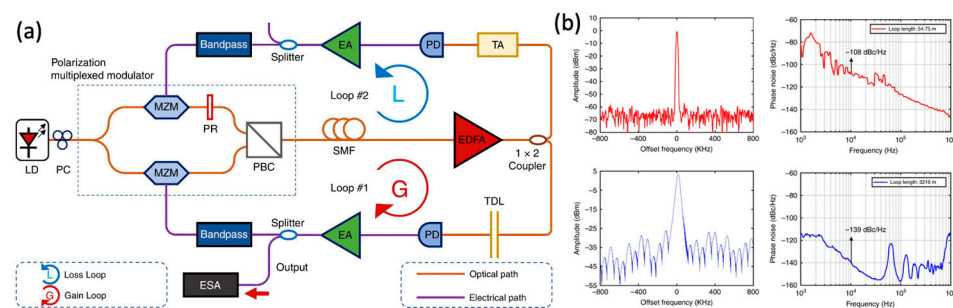


Figure 4. A typical PT-symmetric dual-loop OEO. (a) Schematic diagram of the PT-symmetric OEO. (b) Measured single-mode frequency spectrum and phase noise with different loop lengths. Reprinted with permission from [31].

2.6. Summary and Recent Progress

From the above sections, it can be seen that a single-loop OEO is the basic configuration to achieve a single-frequency oscillation. Dual-loop OEOs incorporate two loops with different lengths. The long loop contributes to a high Q-factor and a low phase noise, and the short loop enables a larger FSR and a high SMSR. So, a dual-loop OEO has the combined advantages of a short loop OEO and a long loop OEO. Nonetheless, a design challenge arises due to the dispersion introduced by the long fiber, which can degrade near-carrier phase noise. This degradation occurs because laser frequency noise is converted into phase noise through fiber dispersion [35]. A trade-off is required when selecting the long fiber length to achieve an optimal phase noise performance.

COEOs and PT-symmetric OEOs are specialized forms of dual-loop OEOs that eliminate the need for long optical fibers while still achieving high Q-factors. In COEOs, a coupled cavity configuration facilitates high-Q oscillation, and, in PT-symmetric OEOs, low-phase-noise radio frequency (RF) signals are generated without relying on narrow EBPFs. However, these advanced designs introduce increased structural complexity and demand precise parameter tuning. For instance, in COEOs, the oscillation frequency of the OEO loop must be an integer multiple of the mode-locked laser loop's FSR, necessitating a carefully coordinated design of the EBPF center frequency and laser loop length. Similarly, achieving PT symmetry requires the precise control over the gain, loss, and coupling ratio between the two loops to intentionally break the PT-symmetric condition for selective mode amplification.

The recent progress of single-frequency OEOs is summarized in Table 1. OEOs with various architectures exhibit unique advantages in enhancing key performance parameters including operating frequency, phase noise and SMSR. In [28], a dual-loop OEO is demonstrated, and the resulted 20-GHz oscillating signal has a 70-dB SMSR owing to the Vernier effect in the dual-loop configuration. The combined use of a 2-km and a 3-km SMF significantly increases the mode spacing within the cavity and reduces the performance requirement for the EBBF in loop. A 94.5-GHz oscillating frequency at the W-band has been successfully generated using a polymer-based MZM in a dual-loop OEO [27]. This modulator is implemented with Thin-Film-Polymer on Silicon (TFPSTM) technology and has a larger bandwidth than a lithium niobate modulator. To implement OEOs at terahertz frequencies, modulators are a crucial challenge. New modulators such as plasmonic modulators should be explored for application in OEOs [27]. In a PT-symmetric OEO [32], a 9.867-GHz RF oscillation with a phase noise of -142.5 dBc/Hz at a 10 kHz offset has been realized, which is attributed to the use of a 9.16 km low-loss optical fiber for the realization of a high Q-factor. Simultaneously, the mode selection challenge posed by the long fiber is overcome by leveraging the PT symmetry. So, a suitable mode selection method under the high-Q condition is an important research area to achieve a stable output with ultra-low phase noise.

Table 1. Performance comparison of single-frequency OEOs.

Method	Key Architecture	Frequency (GHz)	Fiber Length	Phase Noise @ 10 kHz (dBc/Hz)	SMSR (dB)	Ref.	Year
Dual-loop	WDM	20	2 km; 3 km	-120.6	70	[28]	2015
	Balanced PD	11.84	2 m; 2 km	-110	60	[25]	2018
	Polymer-based modulator	94.5	1 km; 2.5 km	-70	40	[27]	2023
High-Q optical resonators	Optical ring resonator	2.137	5 m	-100.54	59	[36]	2018
	MRR w/ frequency stabilization	12.23	NA	-95	55	[37]	2020
	MRR	25.65	NA	-88	49.47	[5]	2023
PT symmetry	DPMZM	6.19	54.75 m; 3.216 km	-139	55	[31]	2018
	Polarization control	9.867	9.166 km	-142.5	NA	[32]	2018
	COEO	10	100 m	-109.1	51.4	[33]	2023
	WDM	4.07	10 km	-118	32	[34]	2024
	Dual-mode optical PM	18	7 km	-133.8	53	[38]	2024

3. Operation Frequency and Stability

To meet various application requirements, OEOs have evolved beyond a single-frequency operation to include frequency-tunable and broadband configurations. The critical performance parameters for microwave sources include the operating frequency, frequency stability, phase noise, and tunability, which directly affect the effectiveness and versatility of the OEOs in diverse scenarios. Frequency-tunable OEOs provide flexibility in selecting operating frequencies, enabling their deployment in dynamic communication networks and adaptive radar systems. Broadband OEOs, on the other hand, can generate signals over a wide range of frequencies, broadening their scope for use in multi-functional platforms.

To enhance the performance of OEOs, particularly in terms of the frequency stability, advanced techniques such as phase-locked loops (PLLs) and injection locking (IL) have also been introduced. PLL-based OEOs achieve improved frequency stability by locking the oscillation frequency to a stable external reference, reducing the drift and ensuring

precise control. Similarly, IL techniques stabilize the oscillation frequency by injecting a highly stable signal into the system, suppressing undesired modes and enhancing the phase noise performance. These approaches not only enhance the reliability of OEOs but also expand their application potential in environments by demanding stringent frequency control, such as satellite communications and secure data links.

3.1. Frequency Stability

3.1.1. Frequency Stability and Influencing Factors

For OEOs, frequency stability is influenced by various factors. First, the high-Q components in OEOs, such as long optical fibers and narrowband electrical filters, are susceptible to environmental influences. Especially, the optical fibers affected by temperature may change the cavity lengths, leading to unstable output frequencies. Additionally, the dispersion and nonlinear effects of the optical fibers also impact the frequency stability. The noises introduced by active components, such as lasers, photodetectors, and amplifiers, also affect the frequency stability. In addition, the multiple modes oscillating in the loop result in multimode noise and mode competition, which can cause issues like mode hopping and drifting, thus affecting the frequency stability. Frequency stability can be described as short-term frequency stability and long-term frequency stability. Phase noise is a frequency-domain representation of short-term frequency stability. Time jitter is a time-domain representation of short-term frequency stability. Allan variance is a time-domain representation of long-term frequency stability.

3.1.2. Methods to Improve Frequency Stability

Enhancing the frequency stability of OEOs involves approaches such as environmental condition control, phase noise suppression, and SMSR enhancement. Temperature control, through temperature-stabilized chambers or temperature-insensitive optical fibers, can mitigate thermal effects [39]. Multi-core optical fibers (MCFs) can create multi-loop OEOs, where co-located loops share the same environmental conditions, reducing the optical fiber length requirements while enhancing the stability [6].

PLL, self-phase-locked loop (SPLL), IL, and self-injection locking (SIL) techniques are widely implemented to further improve the frequency stability. In a PLL, the phase error voltage is derived by comparing the OEO output signal with an external reference, and it is fed back to an electrical phase shifter for phase drift compensation, effectively converting the OEO into a voltage-controlled oscillator (VCO). For example, a PLL-stabilized OEO generating a 2.5 GHz signal with a phase noise of -134 dBc/Hz at a 10-kHz offset frequency significantly reduces Allan deviation and enhances the long-term stability [3]. However, PLL systems are susceptible to phase noise from external reference signals. To address this issue, SPLL uses a delay-line frequency discriminator (DLFD) to generate the error signal. By comparing the delayed OEO output signal with its original, the SPLL achieves phase compensation by controlling the bias voltage of the used MZM in the oscillating loop [40], [41].

On the other hand, the IL enhances the frequency stability of OEOs by synchronizing the oscillation frequency with an external electrical or optical reference signal. In the electrical IL, the oscillation frequency of the OEO is pulled to match the frequency of the injected signal when they are sufficiently close, maintaining a constant phase difference between them [42]. This method minimizes the impact of environmental fluctuations and improves the phase noise performance near the carrier frequency. Additionally, the injected signal amplifies the energy of the locked oscillation mode, enhancing the mode competition and improving the SMSR. For instance, an electrical injection-locked dual OEO operating at a 10 GHz, as described in [43], uses the RF output signal of a high-Q long-fiber master OEO to lock a short-fiber slave OEO. This configuration suppresses the

side modes and preserves the master OEO’s high-Q properties, achieving a phase noise below -110 dBc/Hz at low offset frequencies. Similarly, a COEO employing optical IL couples an external optical reference signal into a mode-locked laser loop [44]. This approach achieves an over 8 dB spur suppression in the RF spectrum. These results highlight the effectiveness of the IL in reducing phase noise and improving the SMSR, making it a vital technique for frequency stabilization in OEOs.

The phase noise performance of OEOs using IL is inherently constrained by the noise of the external source. To address this, the SIL technique has been proposed, wherein a portion of the output oscillation signal is coupled out, delayed, and reinjected into the OEO loop as a locking signal. Low-loss optical fiber delay lines are typically used to counteract the high loss of electrical delay lines; however, the use of long optical fibers reduces the FSR and increases the environmental sensitivity. A dual-loop self-injection locking (DSIL) structure can suppress the side modes and mitigate these challenges [8]. To eliminate the reliance on long optical fibers, a frequency-conversion-based SIL OEO was proposed in [45]. As shown in Figure 5, this method uses a coupler to split the oscillation signal, which is then reinjected into the loop after passing through a frequency conversion filter—an equivalent narrowband filter consisting of a frequency conversion pair and a narrowband intermediate frequency (IF) filter. Although residual phase noise from the local oscillator (LO) persists, it can be minimized by reducing the locking bandwidth or achieving delay matching. This frequency-conversion SIL OEO achieves an SMSR exceeding 70 dB at a 10-GHz oscillation. And the phase noise at the 10-kHz offset frequency is nearly 30 dB lower than traditional injection-locked OEOs under identical experimental conditions, demonstrating substantial improvements in the frequency stability.

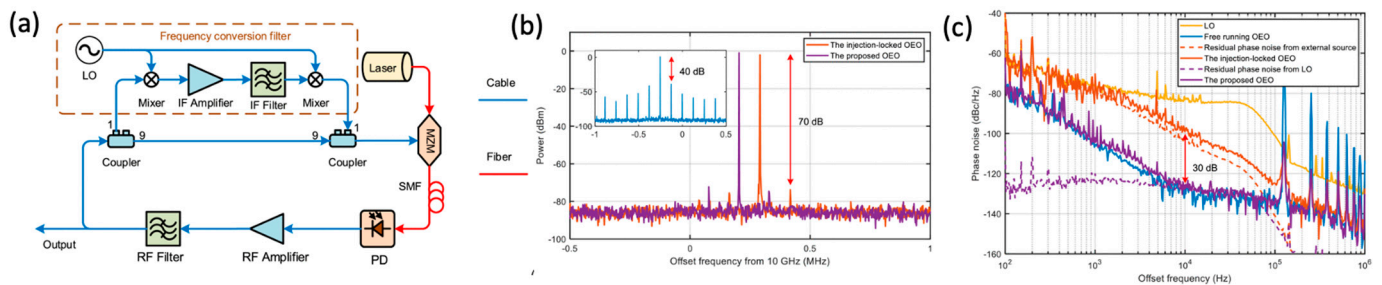


Figure 5. A SIL OEO based on frequency conversion filtering. (a) The scheme of the SIL OEO. (b) The spectrum of the IL OEO and the proposed SIL OEO. (c) Phase noise of the IL OEO and the proposed SIL OEO. Reprinted with permission from [45].

The combination of the PLL, SPLL, IL, and SIL techniques significantly enhances the performance of OEOs by leveraging the strengths of each method. For instance, integrating the PLL and IL enables precise phase compensation and frequency locking, achieving low-phase-noise and high-side-mode suppression ratios, as demonstrated by a 9.5-GHz OEO with a phase noise of -143 dBc/Hz at a 10 kHz offset and an Allan deviation of 1.22×10^{-11} [46]. Similarly, combining the PLL with DSIL reduces the environmental sensitivity and further improves the stability, achieving significant phase noise reductions and Allan deviation improvements compared to the free-running configurations [47]. These results highlight the effectiveness of combining stabilization techniques to meet stringent frequency stability requirements.

3.2. Frequency-Tunable OEOs

A frequency-tunable OEO is capable of adjusting the frequency of its output microwave signal over a defined range, generating high-frequency, broadband-tunable, and

low-phase-noise RF signals. This adaptability makes it a crucial component for advanced applications in communication systems, radar, and electronic warfare. Frequency tuning in OEOs can be achieved using either tunable electrical filters or tunable microwave photonic filters (MPFs) [48,49].

A widely used tunable electrical filter is the Yttrium Iron Garnet (YIG) filter, which allows its center frequency to be adjusted by varying the driving voltage [50,51]. However, YIG filters require precise voltage control, and their tuning range, bandwidth, and anti-interference capability may constrain both the frequency stability and overall tuning performance. These constraints have motivated the exploration of alternative solutions.

Tunable MPFs have emerged as a superior alternative for frequency-tunable OEO designs, offering wider tuning ranges, greater reconfigurability, and stronger anti-interference capabilities. Various MPF-based architectures have been demonstrated. For instance, in an OEO, a tunable single-bandpass MPF has been constructed using a non-sliced broadband optical source (BOS) cascaded with a phase modulator (PM) and a dispersion-compensating fiber (DCF) [52], and frequency tunability in a range of 10.23 to 26.69 GHz was achieved. In another OEO, the MPF was composed of a tunable bandpass optical filter (TBPOF) combined with a PM to provide flexible tuning capabilities from 3.5 to 17.1 GHz [6]. Other approaches involve fiber Bragg grating (FBG)-based structures, including Fabry–Pérot FBGs (FBG-FP) [53], linearly chirped FBGs (LCFBG) [54], and phase-shifted FBGs (PS-FBG) [55–57].

In addition, MPFs based on stimulated Brillouin scattering (SBS) exhibit significant advantages, including high gain and narrowband filtering characteristics [30,58]. For example, an agilely tunable dual-loop OEO utilizing SBS achieves a narrowband MPF through a combination of phase modulation and selective sideband amplification via SBS [59]. The oscillation frequency in this configuration is determined by the frequency of the signal wave, pump wave, and Stokes frequency shift. By adjusting the wavelength of the pump laser, the system achieves a wide frequency tuning range from DC to 60 GHz. The measured SSB phase noise remains stable at approximately -100 dBc/Hz at a 10 kHz offset for all oscillation frequencies, with dual-loop fiber lengths ranging from 2 km to 4 km.

Table 2 provides a summary of the frequency-tuning methods and the characteristics of frequency-tunable OEOs. In terms of the tuning range, MPF-based OEOs demonstrate significant advantages over YIG-based OEOs, achieving tuning ranges of several tens of GHz [53,58]. However, both YIG-based and MPF-based OEOs typically exhibit tuning steps at a MHz level, primarily due to the bandwidth limitations of the tunable electrical filters and tunable MPFs.

Table 2. Performance comparison of frequency-tunable OEOs.

Method	Key Architecture	Frequency Range (GHz)	Phase Noise @ 10 kHz (dBc/Hz)	Ref.	Year
YIG-tuned	multi-loop OEO	6–12	-128 @ all frequency	[50]	2003
	COEO	8–21	-126 @ 15 GHz;	[51]	2021
MPF-tuned	PS FBG and two cascaded PM-based MPFs; single-loop OEO	3–28	-102 @ 10 GHz	[55]	2012
	PS FBG and an MZM-based MPF; single-loop OEO	8.4–11.8	-100 @ 10.6 GHz	[56]	2012
	BOS, PM, and DCF-based MPF; dual-loop OEO	10.23–26.69	-100 @ 15 GHz, 20 GHz, 25 GHz	[52]	2014
	FBG FP and PM-based MPF; dual-loop OEO	3.5–45	-112.93 @ 44.3 GHz;	[53]	2017
	TBPOF and PM-based MPF; dual-loop OEO	3.5–17.1	-100 @ 7.8 GHz	[6]	2018

	BOS, MZM, and LCFBG-based MPF; dual-loop OEO	4.087–13.05	−96.9 @ 6.5 GHz	[54]	2018
	SBS-based MPF; dual-loop OEO	5.34–38.34	−120 @ 100 kHz @ all frequency	[58]	2018
	PS FBG and PM-based MPF; single-loop PT-symmetric OEO	2–12	−128 @ 6 GHz	[57]	2020
	PM and PS FBG-based MPF; Single-loop OEO with an optical phase compensation loop	0.118–24.092	−96.4 @ 18.099 GHz	[60]	2022
MZM as an optical PS-tuned	PT-symmetric dual-loop OEO	1.5 kHz	−108 @ 4.2 GHz	[61]	2020
IL-PLL-tuned	dual-loop COEO	1.76 kHz	−130.04 @ 9.95554 GHz	[4]	2023

Recent advancements have introduced tunable OEOs capable of finer tuning steps at the kHz level. For instance, a frequency-tunable PT-symmetric OEO is reported in [60], where a dual-parallel MZM (DPMZM) functions as an optical phase shifter. By controlling the bias voltage of the parent MZM, the total phase of the OEO loop is adjusted, enabling fine-tuning within a kHz-level range. However, the stability of this design is limited due to its polarization dependence, which is highly sensitive to environmental fluctuations, resulting in poor output signal stability.

A more robust approach is presented in [4], which describes a finely tunable COEO based on the IL and a PLL. By precisely controlling the frequency of the injected signal and adjusting a tunable optical delay line, the system achieves a tuning range of 1.76 MHz with an exceptionally fine tuning step of 10 Hz. Furthermore, this design ensures excellent frequency stability in the output signals, addressing the limitations in polarization-sensitive designs.

3.3. Broadband OEOs

As discussed earlier, frequency-tunable OEOs typically produce single-mode signals with a limited frequency-scanning speed. In contrast, broadband OEOs—such as multi-frequency OEOs and frequency-scanning OEOs—are capable of directly generating multi-frequency signals, chirped signals, or even chaotic signals. These capabilities make broadband OEOs particularly valuable for applications in multi-band communication, radar systems, and electronic interference and countermeasure technologies.

3.3.1. Multi-Frequency OEOs

To address the growing demands for multi-mode and multi-band operations in wireless communication applications [2], significant research has been conducted on multi-frequency OEOs capable of simultaneously generating multiple stable oscillation frequencies. Multi-frequency OEOs are generally categorized into serial-structure multi-frequency OEOs and parallel-structure multi-frequency OEOs.

A typical serial-structure multi-frequency OEO consists of a single loop equipped with a multi-bandpass MPF. The multi-bandpass MPF can be constructed using technologies such as multi-channel optical notch filters (ONFs) [62], FBG-FP filters [63,64], or SBSs [65]. While serial-structure multi-frequency OEOs are relatively simple in design, they are prone to gain competition between oscillation modes, which can lead to instability.

In contrast, parallel-structure multi-frequency OEOs offer a more robust solution by using independent loops for each oscillation frequency [66,67]. This architecture increases the system complexity but allows the gain in each loop to be tuned independently, thus mitigating the gain competition between the frequencies and ensuring stable oscillation.

This design also ensures good phase coherence between the generated signals, making it a preferred choice for applications requiring simultaneous multi-band operation.

A noteworthy example of a parallel-structure design is the broadband random OEO leveraging Rayleigh scattering [68]. This configuration employs distributed Raman amplification to enhance both incident and backscattered light within the feedback loop, creating a distributed random feedback mechanism. Unlike traditional multi-frequency OEOs with fixed cavity lengths, the Rayleigh scattering mechanism eliminates discrete longitudinal modes, enabling continuous broadband frequency oscillations from DC to 40 GHz. The experimental results, as shown in Figure 6b, illustrate the capability of this OEO to generate ultra-wideband microwave signals with a random amplitude and frequency distribution. These characteristics demonstrate the potential of multi-frequency OEOs, not only for wireless communication, but also for noise radar systems, secure communications, and random bit generation.

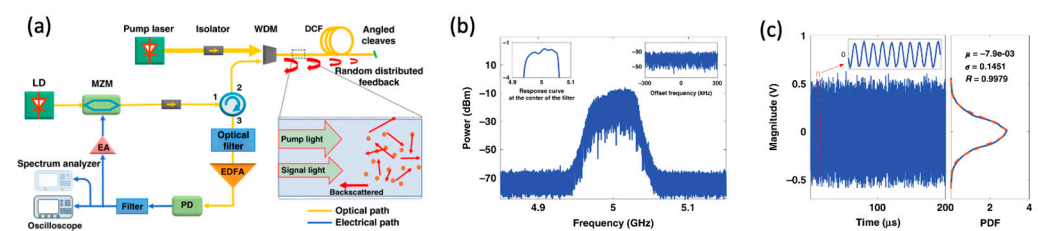


Figure 6. (a) Schematic diagram and operation principle of the broadband random OEO. (b) The electrical spectrum of the generated signals centered at 5 GHz. (c) Temporal waveform and the probability density function of the signal. Reprinted with permission from [68].

By combining robust architectures, such as parallel-structure loops, with innovative mechanisms like Rayleigh scattering, multi-frequency OEOs are poised to meet the demands of next-generation multi-band communication systems, offering both versatility and high performance.

3.3.2. Frequency-Scanning OEOs

In addition to single-frequency microwave signals, OEOs can generate linearly chirped waveforms (LCWMs) through rapid frequency scanning, which are critical for applications in spread-spectrum communication systems and radar systems. Although broadband frequency-tunable OEOs can theoretically produce LCWMs, their frequency-scanning speed is inherently limited. This limitation arises because the OEO operates in an unstable state during frequency tuning, requiring a new oscillation mode to re-establish from noise at each frequency step. This process makes it challenging to directly generate high-quality LCWMs.

To address this issue, frequency-scanning OEOs based on Fourier domain mode locking (FDML) have been proposed. In FDML-based OEOs, a tunable MPF is employed, with center frequency fast scanning. The FDML operation is achieved when the frequency scanning period of the MPF is equal to or a fraction of the round-trip time within the cavity. Under this condition, the OEO operates in a quasi-stationary state, with multiple longitudinal modes spanning the entire scanning range simultaneously excited and sustained within the cavity. By rapidly tuning the MPF, the OEO can directly output a broadband and high-performance LCWM.

Several advanced configurations of FDML-based OEOs have been developed to enhance their performance and flexibility. These include harmonically FDML OEOs [69], dual-chirp FDML OEOs [70], dual-band FDML OEOs [71], and polarization-manipulated FDML OEOs [72,73]. A recent example of an FDML-based OEO [74] demonstrates its ability to overcome the mode-building time limitations during frequency scanning. This

configuration simultaneously excites thousands of longitudinal modes with fixed phase relationships, ensuring a quasi-stationary operation and enabling faster scanning speeds, leading to the generation of LCWMs with a chirp rate of 0.34 GHz/ μ s and a time-bandwidth product (TBWP) of 166,650. The experimental setup employs a tunable MPF synchronized with a periodic driving signal to facilitate continuous frequency sweeping. Figure 7a illustrates the experimental setup, where the synchronization between the MPF and cavity round-trip time ensures a stable FDML operation. The experimental results, shown in Figure 7b,c, highlight the reconfigurability of both the center frequency and tuning range. These results demonstrate the superior performance of the FDML-based OEO, offering broadband frequency scanning and high-quality LCWM generation.

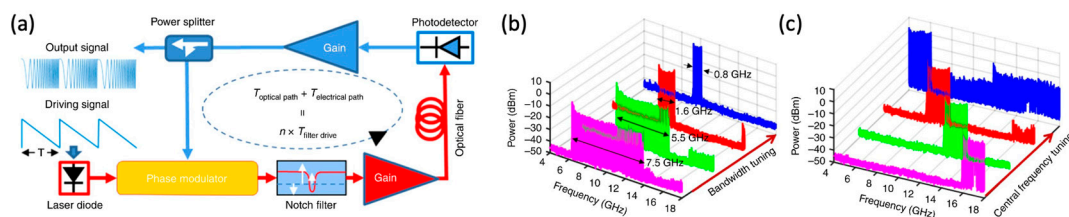


Figure 7. An agilely tunable dual-loop OEO based on SBS. (a) Schematic diagram of the FDML OEO. (b) The scanning range tuned from 0.8 GHz to 7.5 GHz with a central frequency of 10 GHz. (c) The central frequency tuned from 5 GHz to 17 GHz with a scanning range of 2 GHz. Reprinted with permission from [74].

The advancements in FDML-based OEOs not only improve the speed and quality of LCWMs but also broaden their application scope. From radar systems requiring high-speed chirps to secure communications and high-frequency sensing, the demonstrated capabilities of these systems represent a significant step forward in the development of next-generation OEOs.

4. Applications

Owing to the advantages of a low phase noise, high spectral purity, and larger working bandwidth, OEOs with different architectures have been widely applied across various fields, including high-precision sensing and measurement, communication and radar systems, and computational applications. These distinct performance attributes make OEOs highly suitable for systems that demand high-frequency stability and spectral purity, as summarized in Figure 8 and Table 3.

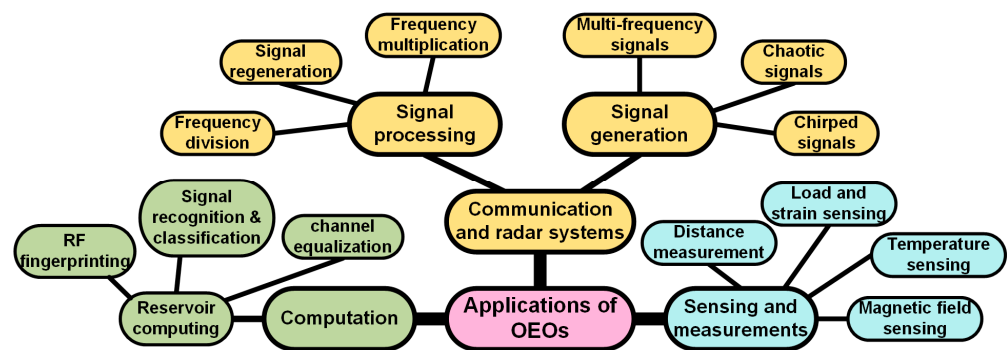


Figure 8. Summary of the main applications of OEOs.

In the realm of sensing and measurement, OEOs are utilized to detect physical quantities by establishing a direct relationship between the measured parameter and the oscillation frequency. For example, a dual-loop OEO has been implemented for magnetic field

sensing, achieving a sensitivity of -16.54 kHz/mT through frequency shifts corresponding to magnetic field variations [75]. Similarly, a COEO has been employed for temperature-compensated Faraday rotation angle measurements, benefiting from its dual-loop configuration to mitigate temperature disturbances. This setup functions effectively as a dual-parameter sensor with sensitivities of 375.73 Hz/deg for the Faraday rotation angle and 1.6 kHz/ $^{\circ}$ C for the temperature changes [76]. These applications demonstrate the OEO's capability to provide accurate and stable measurement solutions in dynamic environments.

In communication and radar systems, OEOs play a vital role in generating the stable, high-frequency signals necessary for advanced functionalities. A notable example is a photonic-assisted joint radar and communication system designed using a single-loop OEO combined with an optical multi-dimensional processing module for intelligent transportation applications. This system achieved a communication capacity of 335.6 Mbps, a range resolution of 0.075 m, and a maximum unambiguous range of 10.725 m under a 2 GHz bandwidth centered at 24 GHz [7]. Another advancement involves an orthogonal frequency division multiplexing (OFDM) radar and communication system, which realized two-dimensional radar imaging with a range resolution of 0.075 m and a communication capacity of 6.4 Gbps. This system notably reduced the error vector magnitude (EVM) from 12.5% to 4.7% under a 125 kHz subcarrier spacing when compared to systems using conventional microwave sources [77]. These examples underscore the OEOs' capability to improve the signal integrity, resolution, and data transmission in high-performance communication and radar systems.

Beyond signal generation, OEOs are also instrumental in advanced signal processing tasks, such as signal regeneration, frequency multiplication, and frequency division. For instance, a linearly chirped microwave signal with a 6.5 GHz center frequency and a 3 GHz bandwidth was injected into a dual-polarization dual-drive Mach–Zehnder modulator (DP-DDMZM)-based OEO. This process resulted in a multiplied output signal with a 26 GHz center frequency and a 12 GHz bandwidth, accompanied by a 20.4 dB improvement in the phase noise relative to the seed signal [20]. Additionally, a single-loop OEO-based optical pulse train (OPT) frequency divider was demonstrated, where the MZM acted as an optical switch to manipulate the repetition rate. This setup enabled frequency division by factors of two and three without degrading the phase noise, making it highly suitable for applications in frequency–time distribution and synchronization systems [78].

The inherent nonlinear effects in OEOs further expand their functional capabilities. Imperfections in SMFs, such as non-uniform internal refractive index distributions, give rise to Rayleigh scattering (RS) and Brillouin scattering (BS). These nonlinear effects can be stimulated using a pump laser, allowing OEOs to adapt more effectively to continuous resonant frequencies. Leveraging these nonlinearities, a random OEO was demonstrated to regenerate continuous ultra-wideband and multi-frequency signals, achieving a signal-to-noise ratio improvement with an SMSR over 35.2 dB and phase noise surpassing -86 dBc/Hz at a 1 kHz offset within a 10 GHz operating bandwidth [79]. Moreover, by adjusting the DC bias of the MZM to operate in the nonlinear region, chaotic signals can be generated, offering promising applications in secure communication and radar systems [80].

In recent years, OEOs have also gained attention in the field of computation, particularly in implementing reservoir computing (RC)—a specialized form of recurrent neural networks. In optoelectronic RC systems, the MZM operating in the nonlinear region serves as a dynamic nonlinear node, while broadband OEOs provide the necessary temporal dynamics. These systems have been successfully applied to tasks such as pattern recognition and time-series prediction [16]. Narrowband OEOs have also proven to be effective alternatives to deep learning systems in resource-constrained edge computing.

For example, a narrowband single-loop OEO-based RC was employed for RF fingerprinting, achieving a remarkable 97% accuracy rate with significantly less training data than conventional neural networks [81]. Similarly, narrowband OEO-based RC systems have been utilized for the recognition and classification of IQ-modulated radio signals, demonstrating the ability to maintain a high accuracy even with limited training data [82].

Table 3. Applications of OEOs with different architectures.

Application	Architecture	Function	Performance	Ref.	Year
Sensing and measurements	Dual-loop OEO	Magnetic field sensing	Sensitivity: -16.54 kHz/mT	[75]	2024
	COEO	Temperature-compensated Faraday rotation angle measurement	Sensitivity of the Faraday rotation angle: 375.73 Hz/deg; sensitivity of the temperature: 1.6 kHz/ $^{\circ}$ C	[76]	2024
Communication and radar systems	Single-loop OEO with an optical multi-dimensional processing module	A joint radar and communication system	Communication capacity: 335.6 Mbps; range resolution: 0.075 m; maximum unambiguous range: 10.725 m	[7]	2021
	Single-loop OEO	An orthogonal frequency division multiplexing radar and communication joint system.	Communication capacity: 6.4 Gbps; range resolution: 0.075 m; maximum unambiguous range: 300 m	[77]	2022
	Single-loop broadband OEO	A chaotic radar ranging system	Ranging resolution: 1.4 cm	[80]	2023
Signal processing	Single-loop OEO based on injection locking	Improving the quality of arbitrary periodic waveforms	Phase noise improvement: beyond 15 dB; SNR improvement: around 20 dB.	[19]	2024
	Single-loop random OEO based on injection locking	Regenerating continuous wideband signals	SMSR beyond 35.2 dB	[79]	2024
	Single-loop OEO with a dual-polarization dual-drive MZM	Frequency multiplication	Generating frequency-quadrupled LCWM: bandwidth, 12 GHz; center frequency, 26 GHz; phase noise reduced by 20.4 dB	[20]	2024
	Single-loop OEO	Optical pulse train (OPT) frequency divider	Frequency division factors: 2 and 3 ; phase noise remained unchanged	[78]	2024
	Single-loop narrowband OEO	Reservoir computing for radiofrequency fingerprinting	Accuracy rate: 97%	[81]	2022
Computing	Single-loop narrowband OEO	Reservoir computing for the recognition and classification of IQ-modulated radio signals	Overall accuracy: 61.7% using 600 training examples	[82]	2024

5. Integrated Optoelectronic Oscillators: Advances and Challenges

Classical OEO designs have historically relied on discrete components, including long optical fiber delay lines and electrical bandpass filters, while being effective at achieving a low phase noise. These designs are inherently bulky due to the length of the fiber required to achieve high Q-factors, and they are often power-hungry, limiting their scalability and practical applications in modern communication systems like 5G and 6G networks [17,83]. Furthermore, the reliance on discrete electrical and optical components limits the potential for system miniaturization and scalability, thus posing a significant

challenge, as modern applications demand more compact, power-efficient, and integrated solutions [84,85].

Recent advances in photonic integration have offered a promising solution to these limitations, enabling the development of integrated OEOs. These integrated designs combine key components—such as modulators, resonators, and detectors—onto a single chip, resulting in systems that are not only smaller and more power-efficient but also capable of tunable performance across a wide frequency range. Moreover, integrated OEOs leverage novel filtering techniques, such as PT-symmetry and microring resonators, to achieve single-mode oscillation and wideband tunability without relying on large external filters [86,87]. For example, integrated designs have demonstrated tunability across a broad frequency range up to 42.5 GHz, which surpasses many traditional designs [88]. This section reviews the transition from classical to integrated OEOs, highlighting key technological achievements in the field and examining the ongoing challenges that researchers and engineers face in further refining these systems.

5.1. Achievements in Integrated OEO Designs

The integration of OEOs onto photonic platforms is critical for improving the performance, scalability, and energy efficiency. Several integration platforms have been explored, each offering distinct advantages and limitations based on the material properties, fabrication complexity, and application requirements. Table 4 summarizes the comparison of major integration platforms, including silicon photonics (Si), indium phosphide (InP), silicon nitride (Si_3N_4), and hybrid integration.

Silicon Photonics (Si): Silicon photonics is a widely adopted platform due to its compatibility with CMOS fabrication processes, allowing for mass production and reduced costs. It offers a high integration density and excellent scalability, making it suitable for compact OEO designs. However, silicon's weak electro-optic properties and lack of efficient light generation limit its performance in applications requiring high-speed modulation and on-chip light sources.

Indium Phosphide (InP): InP-based integration offers native light generation through on-chip laser diodes and high-speed modulation due to its direct bandgap properties. This platform is ideal for high-frequency OEOs but presents challenges in large-scale integration and higher fabrication costs compared to silicon photonics. Thermal management and device reliability also require careful consideration.

Silicon Nitride (Si_3N_4): Silicon nitride provides ultra-low optical loss and high-Q resonator performance, making it well-suited for applications demanding a low phase noise and high-frequency stability. Its limited electro-optic properties restrict active component integration, often requiring external modulators or hybrid approaches for active functionality.

Lithium Niobate (LiNbO_3): Known for its excellent electro-optic properties and high optical transparency, lithium niobate is well-suited for high-speed modulators in OEOs. Recent advances in thin-film lithium niobate (TFLN) technology have enabled compact, high-performance photonic devices. However, challenges remain in achieving seamless integration with silicon photonics due to lattice mismatches and fabrication complexity. Hybrid integration techniques and direct bonding methods have been explored to overcome these issues, enabling high-speed and low-loss OEOs.

Graphene and 2D Materials: Graphene and other two-dimensional materials exhibit extraordinary electrical, thermal, and optical properties, making them promising candidates for ultrafast modulation and photodetection in OEOs. However, challenges such as material uniformity, large-scale production, and integration with existing photonic platforms hinder their practical deployment. Advances in chemical vapor deposition (CVD)

techniques and transfer methods are being developed to address these scalability and integration issues.

Hybrid Integration: Hybrid integration combines the strengths of different materials (e.g., Si with InP or LiNbO₃) to leverage their complementary properties. For example, silicon photonics can be integrated with InP lasers for efficient light generation and high-speed modulation. While hybrid integration improves the performance versatility, it introduces additional complexity in fabrication and alignment, potentially impacting the scalability and cost.

Table 4. Comparison of integration platforms/material for OEOs.

Platform	Advantages	Limitations	Applications	Potential Solutions
Si	CMOS compatibility, low-cost, scalable	Poor light generation, limited electro-optic effect	Compact OEOs, large-scale integration	Hybrid integration with InP or LiNbO ₃ for active components
InP	On-chip lasers, high-speed modulation	High cost, limited scalability, thermal issues	High-frequency OEOs, telecom systems	Improved thermal management, optimized fabrication processes
Si ₃ N ₄	Ultra-low optical loss, high-Q resonators	Limited active functionality	Ultra-low-phase-noise OEOs	Hybrid integration with InP, LiNbO ₃ for active functions
LiNbO ₃	High electro-optic coefficient, low optical loss	Fabrication complexity, limited CMOS compatibility	High-speed modulators, low-phase-noise OEOs	Thin-film LiNbO ₃ , direct bonding with silicon photonics
Graphene and 2D Materials	Ultra-high carrier mobility, broadband absorption, tunability	Scalability, material uniformity, integration challenges	Ultrafast modulators, broadband OEOs	Advanced CVD techniques, improved transfer methods
Hybrid Integration	Combines material advantages, flexible designs	Complex fabrication, alignment challenges	Broadband, high-performance OEOs	Photonic integration platforms with optimized packaging

Recent innovations have resulted in significant advancements in integrated OEO technologies. One of the most notable is the monolithic integration of OEO components on a SiGe BiCMOS silicon photonic platform, which achieved a phase noise of -115 dBc/Hz at a 100 kHz offset from a 750 MHz signal. This design drastically reduced the system size and power consumption compared to traditional discrete-component designs [89]. Another example of monolithic integration is the use of silicon photonic platforms to achieve a wide frequency tuning range from 3 GHz to 7 GHz with a phase noise of -80 dBc/Hz at a 10 kHz offset, showing the potential for low-cost, scalable OEOs for high-frequency applications [84]. Moreover, the use of directly modulated dual-mode lasers in integrated OEOs has allowed for tunable generation of microwave signals from 28 GHz to 41 GHz, with a phase noise of -106 dBc/Hz, showcasing the potential of integrated designs for higher-frequency applications [85]. Another notable development includes the use of a tunable optoelectronic oscillator based on a dual-frequency semiconductor laser, which demonstrated tunability from 14.2 GHz to 25.2 GHz and a phase noise of -106.363 dBc/Hz at a 10 kHz offset [90].

5.1.1. Si-Based OEOs

The silicon microring-based OEO presents a novel approach to microwave signal generation, leveraging the compactness and integrability of silicon photonics. This

architecture combines a laser source, an intensity modulator, and a silicon add-drop MRR to generate wideband tunable microwave signals through direct intensity-modulation-to-microwave conversion. The silicon microring acts as an optical bandpass filter, selecting a single sideband of the modulated signal, which subsequently beats with the laser source to produce the desired microwave frequency. At the same time, the enhanced resonance effect leads to the significant suppression of phase noise due to the prolonged photon lifetime within the resonator. This improvement is attributed to the tight confinement of light and reduced scattering losses in high-Q resonators, which stabilize the oscillation mode and mitigate phase fluctuations. By tuning the wavelength separation between the laser and the resonance of the ring resonator [91], this OEO achieves a frequency tuning range from 5.9 GHz to 18.2 GHz—which is the widest range reported for silicon-based OEOs to date.

As shown in Figure 9a, this design demonstrates exceptional phase noise performance, achieving -110 dBc/Hz at a 1 MHz offset across the tuning range. The microring resonator, fabricated using silicon-on-insulator (SOI) technology, offers a high optical quality factor ($Q \sim 8.1 \times 10^4$), which is critical for improving the purity and stability of the generated signals. Moreover, the tunability is achieved through the thermal control of the ring resonator or by sweeping the laser wavelength, providing a flexible and efficient frequency selection mechanism.

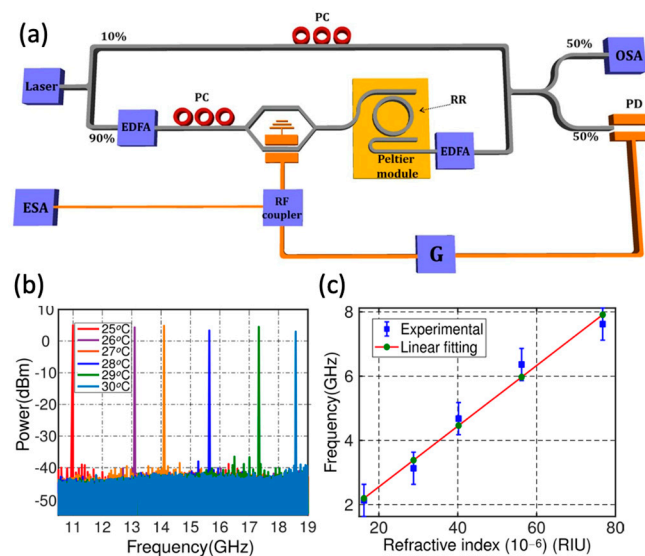


Figure 9. (a) Experimental setup employed for the demonstration of the Si-based tunable OEO. (b) Oscillation frequency simultaneously collected for each setting temperature point. (c) Calculation of the oscillation change depending on refractive index variation. Reprinted with permission from [91].

The proposed silicon OEO also extends its functionality into sensing applications. By monitoring the oscillation frequency shifts corresponding to variations in the ring’s resonance, it achieves a refractive index sensitivity of 94,350 GHz/RIU, with a detection limit as low as 10^{-8} RIU. These results highlight the potential of silicon microring-based OEOs in microwave generation and photonic sensing, paving the way for advanced applications in radar, communication systems, and lab-on-a-chip technologies.

Another notable advancement presents a silicon photonic chip-based Fourier-domain mode-locked optoelectronic oscillator (FDML-OEO) capable of generating independently tunable LCMWs [92,93]. This system integrates dual racetrack MRRs with metallic micro-heaters, enabling precise thermal control over the resonance wavelengths. The dual MRR-based microwave photonic filters serve as narrowband optical filters, shaping the optical signals before the photodetection [93]. By exploiting the FDML principle,

where the scanning period of the MPF matches the cavity round-trip time, the system maintains continuous oscillation without the need to rebuild modes from noise. This configuration allows for wide frequency tunability ranging from 7.5 GHz to 12.5 GHz, with customizable chirp rates in each frequency band.

The exceptional performance of this integrated OEO design stems from the combination of high-Q MRRs for effective mode selection and the thermal tunability of silicon waveguides for dynamic frequency control. The high Q-factor of the MRRs enhances signal purity by suppressing unwanted side modes, while the FDML mechanism enables stable, rapid frequency sweeps without compromising the signal integrity. Additionally, the silicon photonic platform offers low optical losses and scalability, contributing to improved energy efficiency and compact integration. However, challenges such as thermal tuning latency and nonlinear effects in silicon waveguides may impact the system’s long-term stability. Addressing these issues requires advanced thermal management strategies and optimized waveguide designs to fully leverage the benefits of silicon-based OEO systems in high-performance radar and communication applications [94].

5.1.2. Integrated PT Symmetric OEOs

Recent advancements in integrated OEOs have demonstrated the significant potential of PT-symmetric designs for enhancing mode selection and frequency tunability. In [87], Ahmadfard and Hosseini presented a novel design of a tunable PT-symmetric OEO that integrated essential components such as an MRR with a high Q-factor and an adjustable optical power splitter, as shown in Figure 10a. The operation of the proposed PT-symmetric OEO relied on the interaction between two coupled feedback loops. Each loop is geometrically identical, with one providing gain and the other loss. As explained in Section 2.5, the PT symmetry is achieved when the gain and loss coefficients are balanced. As the symmetry is broken, a single mode with higher gain dominates, while other modes are suppressed, resulting in a stable single-mode oscillation. The system incorporates a tunable MPF based on the integrated MRR to provide precise control over the generated microwave frequency.

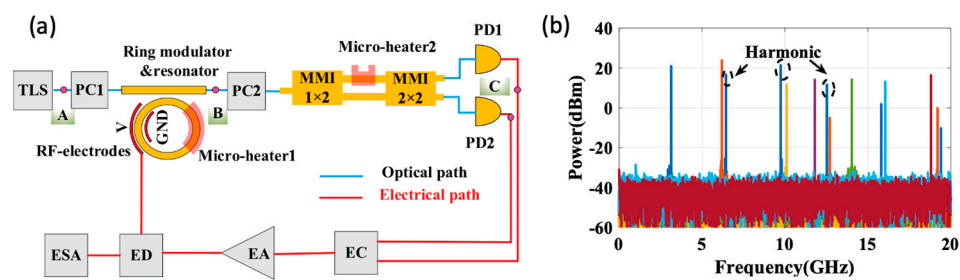


Figure 10. (a) Schematic diagram of the proposed integrated PT-symmetric OEO. (b) Frequency tunability of the proposed PT-symmetric OEO. Reprinted with permission from [87].

The SSB phase noise of the proposed OEO was calculated at the following two frequencies: 6.2 GHz and 11.5 GHz. The phase noise at a 10 kHz offset was measured as -79.22 dBc/Hz at 6.2 GHz and -76.5 dBc/Hz at 11.5 GHz. The SMSR was approximately 40 dB, indicating stable single-mode operation without the need for an additional microwave filter. The balanced gain and loss mechanism allows for selective mode amplification, leading to a high spectral purity and an improved SMSR. This behavior directly correlates with the system’s ability to suppress the side modes. By tuning the laser wavelength, the oscillation frequency can be varied from 0 to 20 GHz, covering a wide range of potential applications. The stability of the system is maintained through the precise

control of the gain and loss within the two feedback loops, which are adjusted using micro-heaters integrated into the power splitter.

Another notable development is the on-chip tunable PT-symmetric OEO fabricated on a SOI platform [95]. This design integrates a high-Q MRR, a PT-symmetric mode-selective architecture based on an MZI, and high-speed PDs on a single chip. By carefully balancing the gain and loss in two mutually coupled optoelectronic loops through the precise control of the MZI phase shift, stable single-mode oscillation was achieved without the need for long optical fibers. The device exhibited a wide frequency tunability from 0 to 20 GHz and demonstrated an excellent phase noise performance of -80.96 dBc/Hz at a 10 kHz offset for a 13.67 GHz oscillation frequency, along with a high SMSR of 46 dB.

The integration of PT-symmetric structures into OEOs fundamentally enhances the mode selection by exploiting the PT-symmetry breaking, where gain and loss are balanced across coupled loops. Additionally, the combination of the PT symmetry with a tunable MPF based on a microring resonator enables continuous frequency tuning and further suppresses the side modes. The on-chip implementation reduces the system complexity, enhances the robustness, and paves the way for fully integrated, compact, and low-power OEOs suitable for next-generation radar, communication, and sensing applications.

5.1.3. Hybrid Integrated OEOs

Hybrid integrated OEOs have emerged as a promising solution to address the challenges of size, cost, and performance in traditional OEO designs. By combining the strengths of multiple material platforms to overcome the limitations of single-material designs as well as photonic integration with advanced packaging techniques, this integration enables superior performance in phase noise reduction, frequency tunability, and signal stability. A critical advantage of hybrid integration lies in the optimized balance between low-loss passive components and high-efficiency active devices, leading to enhanced oscillator performance. A notable example of this approach is the hybrid-integrated wideband tunable OEO, which integrates a distributed feedback (DFB) laser chip with a silicon photonic chip and electronic components through microstrip interconnections [96].

As shown in Figure 11a, this hybrid design incorporates a polarization-maintaining fiber ring as the high-Q optical energy storage element, enabling the generation of ultra-low-phase-noise microwave signals. The architecture also features a YIG filter for frequency tuning. The filter is controlled via an external magnetic field to provide a wide tunability range from 3 GHz to 18 GHz, covering the essential frequency bands such as C, X, and Ku, which are critical for radar and communication systems. The experimental results demonstrate a phase noise of -128.04 dBc/Hz at a 10 kHz offset for a 10 GHz signal. The low phase noise is primarily attributed to the high-Q Si_3N_4 resonator, which provides narrow linewidth filtering, suppressing phase fluctuations by extending the photon lifetime. Concurrently, the InP DFB laser offers efficient optical gain, ensuring a stable oscillation mode with minimal intensity noise.

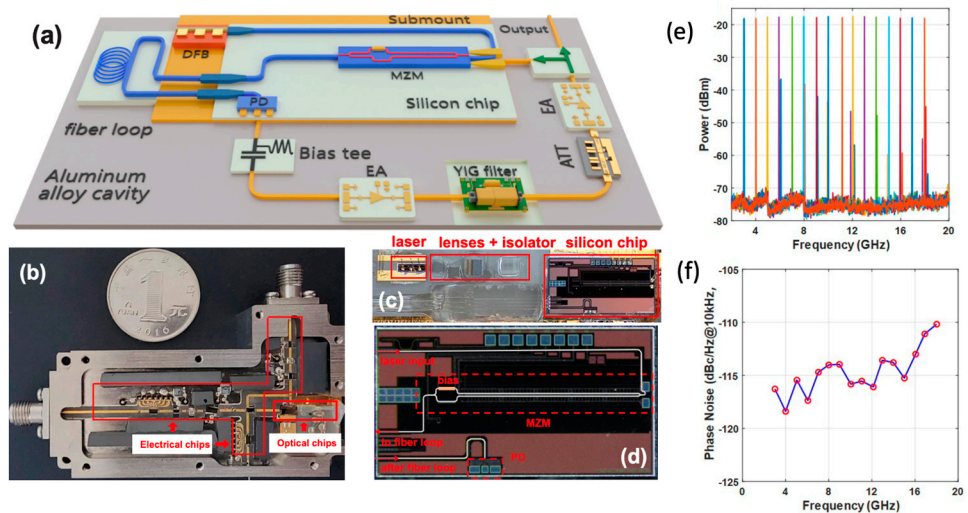


Figure 11. (a–d) Schematic and micrographs of the hybrid integrated OEO. (e) Super-imposed spectrum with a frequency tuning step of 1 GHz. (f) Measured phase noise at a 10-kHz offset frequency of different oscillation frequencies. Reprinted with permission from [96].

The hybrid structure leverages advanced silicon photonic components, including a high-speed MZM and a germanium-doped PD, to ensure efficient modulation and a wide operational bandwidth. These optical and electronic chips are packaged into an aluminum alloy cavity with dimensions of 3 cm × 7 cm × 1.4 cm, thus significantly reducing the physical footprint. Moreover, a temperature control system is employed to mitigate thermal fluctuations, improving the long-term frequency stability. The inclusion of the YIG filter further enhances the OEO’s tuning capability while maintaining superior phase noise characteristics.

5.2. Comparison of Current Methods

The performance of integrated OEOs has come to rival, and, in some cases, surpass, traditional OEOs in terms of the frequency tunability and phase noise. Traditional OEOs rely heavily on long fiber delay lines to achieve low phase noise, but this comes with trade-offs in system size and frequency agility [17,84]. Integrated OEOs, on the other hand, achieve similar or better phase noise performance while significantly reducing the size and power consumption. For example, an all-optical gain OEO, which eliminates the need for traditional electrical amplifiers, has achieved a tuning range of 14.2 GHz to 25.2 GHz while maintaining a low phase noise [90]. In comparison, a traditional fiber-based OEO design would struggle to achieve such a tuning range without becoming impractically large and power-hungry.

Additionally, integrated designs have introduced innovations such as PT symmetry, which improves the mode selection and stability. A PT-symmetric OEO, based on a dual-wavelength approach, achieved tunability from 1 GHz to 22 GHz and phase noise ranging from −122 to −130 dBc/Hz at a 10 kHz offset [86]. Such advancements in integrated designs offer a promising alternative to traditional configurations, particularly for applications requiring compact, power-efficient solutions. Table 5 shows a comparison among various research works since 2017 (partially integrated and compact OEOs). Early silicon-based designs achieved a phase noise of −80 dBc/Hz at 5.4 GHz [84], while InP-based dual-mode lasers extended the frequency range to 37.5–43.59 GHz, with an improved phase noise of −94.87 dBc/Hz [97]. Innovations in PT-symmetric architectures have further pushed the boundaries, with silicon microring resonators (MDRs) and PS-FBGs achieving phase noise levels of −124 dBc/Hz and −125 dBc/Hz across 2–12 GHz and 1–22 GHz, respectively [98], [86]. Most recently, hybrid integration techniques achieved a record phase noise of −128.04

dBc/Hz over a 3–18 GHz range [96], while a PM + MRR configuration in 2024 offered the widest tuning range of 3–42.5 GHz with a phase noise of -93 dBc/Hz [88]. Furthermore, The Ka-band TFLN-integrated OEO achieved high-frequency operation with a fixed frequency at 30 GHz and a tunable range of 20–35 GHz, demonstrating an excellent phase noise performance of -112 dBc/Hz at a 10 kHz offset, enabled by the monolithic integration of high-Q microring resonators and efficient modulators on a compact TFLN platform [99]. The wide tuning range was achieved by exploiting the high-speed electro-optic modulation capability of LiNbO₃ and the compact, low-loss filtering provided by the silicon photonic circuit. The frequency agility of this design is directly related to the high modulation efficiency of LiNbO₃, which enables rapid tuning with minimal signal degradation. These advancements underscore the potential of integrated OEOs for next-generation communication and sensing applications. And the demonstrated design exemplifies the potential of hybrid-integrated OEOs in meeting the stringent requirements of next-generation radar, wireless communication, and electronic warfare applications.

Table 5. Performance comparison of emerging integrated OEOs.

Key Architectures	Frequency (GHz)	Phase Noise (dBc/Hz)	Offset (Hz)	Ref.	Year
Silicon	5.4	-80	10k	[84]	2017
Dual-mode InP laser	37.5–43.59	-94.87	10k	[97]	2017
DML on InP	2.2–19.5	-110	10k	[100]	2018
DML	8.87	-92	1M	[18]	2018
Multi-section DFB on InP	20.3	-115.3	10k	[101]	2019
Dispersion w/ PT symmetry	16–30	-116	10k	[102]	2020
Silicon MDR w/ PT symmetry	2–12	-117.3	10k	[103]	2020
PS-FBG w/ PT symmetry	2–12	-124	10k	[98]	2020
BiCMOS	0.75	-115	100k	[89]	2021
SiN MDR w/ PT symmetry	3–20	-120	10k	[104]	2021
Cascaded PS-FBGs w/ PT symmetry	1–22	-125	10k	[86]	2021
MLL on InP	24–25	-108	10k	[105]	2021
SOI	4–19	NA	NA	[106]	2022
Hybrid integration	3–18	-128.04	10k	[96]	2023
SOI	7.2–13.2	NA	NA	[107]	2023
PM + MRR	3–42.5	-93	10k	[88]	2024
TFLN	20–35	-110	10k	[99]	2024

6. Discussion and Conclusions

This review has traced the evolution of OEOs, from traditional designs reliant on long fiber loops to emerging integrated systems leveraging advanced photonic technologies. OEOs have proven to be versatile tools for generating high-frequency, low-phase-noise microwave and millimeter-wave signals, making them indispensable in applications ranging from radar and communications to sensing and precision instrumentation. The transition to integrated OEOs marks a significant milestone, enabling compact, power-efficient, and tunable architectures without sacrificing performance. However, these advancements bring new challenges and opportunities for future research.

One of the key challenges facing OEOs is further reducing the phase noise, especially for ultra-precise applications such as satellite communications and quantum systems. Dispersion in optical fibers and nonlinearity in modulators continue to hinder progress in minimizing noise levels. Moreover, achieving the full integration of OEO components, including high-Q resonators, tunable filters, and modulators, remains a formidable technical hurdle. Integrated designs also face thermal sensitivity and polarization stability issues, which must be addressed to ensure reliable operation in practical environments.

Another critical area is enhancing the frequency tunability and stability. While significant strides have been made in developing wideband frequency-tunable and broadband OEOs, maintaining a high spectral purity and low phase noise across the tuning range remains challenging. Advanced designs, such as PT-symmetric OEOs and coupled-loop architectures, have shown promise in addressing these issues, but further refinement is necessary to achieve optimal performance. For multi-frequency and frequency-scanning OEOs, overcoming gain competition and ensuring phase coherence remain important directions for future work.

Although detailed power consumption data are not consistently reported across the studies reviewed, it is important to note that the total energy efficiency of OEO systems depends on both photonic integration and the associated electronic subsystems. Components such as high-speed modulators, optical amplifiers, and feedback control circuits contribute to the overall power budget. While integrated OEOs reduce the physical footprint and optical losses, the additional electronic drivers and amplifiers must be considered for a comprehensive assessment of system performance. Future research should prioritize reporting detailed power consumption metrics to facilitate more accurate comparisons between OEO designs and to guide the development of more energy-efficient architectures.

Looking ahead, advancements in materials, such as silicon nitride and lithium niobate, offer opportunities for improving the environmental stability and device integration. The application of machine learning for adaptive control and optimization could enhance the performance of multi-frequency and broadband OEOs. Moreover, the development of application-specific designs tailored to fields such as radar, optical communications, and quantum information systems will continue to expand the versatility of OEOs. By addressing these challenges, OEOs can realize their full potential, enabling transformative advancements in next-generation communication, sensing, and radar systems.

Author Contributions: Resources and Review, Q.L. and J.P.; Project Administration and Supervision, J.Y. All authors contributed to data analysis and manuscript writing. All authors have read and agreed to the published version of the manuscript.

Funding: This work was supported by the National Natural Science Foundation of China (NSFC) under Grant Nos. 61771029 and 61201155.

Data Availability Statement: No new data were created or analyzed in this study. Data sharing is not applicable to this article.

Conflicts of Interest: The authors declare no conflicts of interest.

References

1. Yao, X.S.; Maleki, L. Optoelectronic microwave oscillator. *JOSA B* **1996**, *13*, 1725–1735. <https://doi.org/10.1364/JOSAB.13.001725>.
2. Yao, X.S.; Maleki, L. Optoelectronic oscillator for photonic systems. *IEEE J. Quantum Electron.* **1996**, *32*, 1141–1149.
3. Spencer, D.T.; Srinivasan, S.; Bluestone, A.; Guerra, D.; Theogarajan, L.; Bowers, J.E. A low phase noise dual loop optoelectronic oscillator as a voltage controlled oscillator with phase locked loop. In Proceedings of the 2014 IEEE Photonics Conference, San Diego, CA, USA, 12–16 October 2014; pp. 412–413. Available online: <https://citeseerx.ist.psu.edu/document?repid=rep1&type=pdf&doi=5e3e6084fe6b5d448a2c803c6e57c4f2f8f3466f> (accessed on 17 November 2024).

4. Qiu, J.; Wei, B.; Yang, L.; Jin, X. Finely Tunable Coupled Optoelectronic Oscillator Based on Injection Locking and Phase Locked Loop. *J. Light. Technol.* **2023**, *41*, 5863–5869.
5. Cui, T.; Liu, D.; Liu, F.; Zhang, Z.; Tang, Z.; Cui, N.; Pan, S. Tunable optoelectronic oscillator based on a high-Q microring resonator. *Opt. Commun.* **2023**, *536*, 129299. <https://doi.org/10.1016/j.optcom.2023.129299>.
6. Huang, L.; Deng, L.; Fu, S.; Tang, M.; Cheng, M.; Zhang, M.; Liu, D. Stable and compact dual-loop optoelectronic oscillator using self-polarization-stabilization technique and multicore fiber. *J. Light. Technol.* **2018**, *36*, 5196–5202.
7. Xue, Z.; Li, S.; Xue, X.; Zheng, X.; Zhou, B. Photonics-assisted joint radar and communication system based on an optoelectronic oscillator. *Opt. Express* **2021**, *29*, 22442–22454.
8. Zhang, L.; Poddar, A.; Rohde, U.; Daryoush, A. Analytical and experimental evaluation of SSB phase noise reduction in self-injection locked oscillators using optical delay loops. *IEEE Photonics J.* **2013**, *5*, 6602217.
9. Bian, Y.; Hirokawa, T.; Lee, W.S.; Chandran, S.; Giewont, K.; Aboketaf, A.; Liu, Q.; Sporer, R.; Rakowski, M.; Dezfulian, K. 300-mm monolithic CMOS silicon photonics foundry technology. *CLEO Appl. Technol.* **2024**, ATu3H-1. https://doi.org/10.1364/CLEO_AT.2024.ATu3H.1.
10. Hirokawa, T.; Bian, Y.; Giewont, K.; Aboketaf, A.; Chandran, S.; Cho, J.-K.; Chowdhury, Z.; Lee, W.S.; Liu, Q.; Sharma, P. Latest progress and challenges in 300 mm monolithic silicon photonics manufacturing. In Proceedings of the Optical Fiber Communication Conference, San Diego CA, USA, 24–28 March 2024; Optica Publishing Group: Washington, DC, USA, 2024; p. Th3H-2. Available online: <https://opg.optica.org/abstract.cfm?uri=ofc-2024-Th3H.2> (accessed on 24 November 2024).
11. Liu, Q.; Aboketaf, A.; Pal, S.; Mosleh, S.; Banihashemian, S.F.; Pavadai, S.; Lee, J.-C.; Bian, Y.; Gong, M.; Orner, B. High-Power Micro-Ring Modulator and Multi-Channel Coupled Ring Resonator for WDM Design on a 300-mm Monolithic Foundry Platform. In Proceedings of the 2024 Optical Fiber Communications Conference and Exhibition (OFC), San Diego CA, USA, 24–28 March 2024; pp. 1–3. Available online: <https://ieeexplore.ieee.org/abstract/document/10526519/> (accessed on 24 November 2024).
12. Zou, F.; Zou, L.; Yang, B.; Ma, Q.; Zou, X.; Zou, J.; Chen, S.; Milosevic, D.; Cao, Z.; Liu, H. Optoelectronic oscillator for 5G wireless networks and beyond. *J. Phys. Appl. Phys.* **2021**, *54*, 423002. <https://doi.org/10.1088/1361-6463/ac13f2>.
13. Liu, Q.; Ge, J.; Fok, M.P. Microwave photonic multiband filter with independently tunable passband spectral properties. *Opt. Lett.* **2018**, *43*, 5685–5688. <https://doi.org/10.1364/OL.43.005685>.
14. Wu, T.; Jiang, Y.; Ma, C.; Jia, Z.; Bai, G.; Zi, Y.; Huang, F. Simultaneous Triangular Waveform Signal and Microwave Signal Generation Based on Dual-Loop Optoelectronic Oscillator. *IEEE Photonics J.* **2016**, *8*, 1–10. <https://doi.org/10.1109/JPHOT.2016.2626007>.
15. Yan, J.; Liang, A.; Xin, F.; Liu, Q. An Optical Microwave Generator based on Stimulated Brillouin Scattering with Fine Tunability. In Proceedings of the Conference on Lasers and Electro-Optics, San Jose, CA, USA, 13–18 May 2018; Optica Publishing Group: Washington, DC, USA, 2018; p. JW2A.181. https://doi.org/10.1364/CLEO_AT.2018.JW2A.181.
16. Li, M.; Hao, T.; Li, W.; Dai, Y. Tutorial on optoelectronic oscillators. *APL Photonics* **2021**, *6*, 061101. <https://doi.org/10.1063/5.0050311>.
17. Hao, T.; Liu, Y.; Tang, J.; Cen, Q.; Li, W.; Zhu, N.; Dai, Y.; Capmany, J.; Yao, J.; Li, M. Recent advances in optoelectronic oscillators. *Adv. Photonics* **2020**, *2*, 044001.
18. Tang, J.; Hao, T.; Li, W.; Domenech, D.; Baños, R.; Muñoz, P.; Zhu, N.; Capmany, J.; Li, M. Integrated optoelectronic oscillator. *Opt. Express* **2018**, *26*, 12257–12265. <https://doi.org/10.1364/OE.26.012257>.
19. Liu, M.; Liu, S.; Yang, L.; Du, C.; Liu, H.; Pan, S. Improving the Quality of Arbitrary Periodic Waveform via Injection-Locking of an Optoelectronic Oscillator. *IEEE Trans. Microw. Theory Tech.* **2024**, *72*, 6678–6685. <https://doi.org/10.1109/TMTT.2024.3406430>.
20. Zhang, W.; Liu, Y.; Wang, B. Low-Phase-Noise Ultra-Wide Arbitrary Waveforms Generation Using a Wideband Injection-Locked Optoelectronic Oscillator. *J. Light. Technol.* **2024**, *42*, 7693–7702. <https://doi.org/10.1109/JLT.2024.3371669>.
21. Zhou, P.; Pan, S.; Zhu, D.; Guo, R.; Zhang, F.; Zhao, Y. A Compact Optoelectronic Oscillator Based on an Electroabsorption Modulated Laser. *IEEE Photonics Technol. Lett.* **2014**, *26*, 86–88. <https://doi.org/10.1109/LPT.2013.2289937>.
22. Zhao, S.; Yan, J. Low phase noise optoelectronic oscillator based on an electroabsorption modulated laser. *Appl. Opt.* **2019**, *58*, 4512–4517. <https://doi.org/10.1364/AO.58.004512>.
23. Eliyahu, D.; Maleki, L. Low phase noise and spurious level in multi-loop opto-electronic oscillators. In Proceedings of the IEEE International Frequency Control Symposium and PDA Exhibition Jointly with the 17th European Frequency and Time Forum, 2003. Proceedings of the 2003, Tampa, FL, USA, 4–8 May 2003; pp. 405–410.

24. Leeson, D.B. A simple model of feedback oscillator noise spectrum. *Proc. IEEE* **1966**, *54*, 329–330. <https://doi.org/10.1109/PROC.1966.4682>.
25. Hasanuzzaman, G.K.M.; Kanno, A.; Dat, P.T.; Iezekiel, S. Self-Oscillating Optical Frequency Comb: Application to Low Phase Noise Millimeter Wave Generation and Radio-Over-Fiber Link. *J. Light. Technol.* **2018**, *36*, 4535–4542.
26. Yang, J.; Jin-Long, Y.; Yao-Tian, W.; Li-Tai, Z.; En-Ze, Y. An Optical Domain Combined Dual-Loop Optoelectronic Oscillator. *IEEE Photonics Technol. Lett.* **2007**, *19*, 807–809. <https://doi.org/10.1109/LPT.2007.897290>.
27. Hasanuzzaman, G.K.M.; Iezekiel, S.; Kanno, A. 94.5 GHz Dual-loop Optoelectronic Oscillator. In Proceedings of the 2023 International Conference on Electrical, Computer and Communication Engineering (ECCE), Chittagong, Bangladesh, 23–25 February 2023; pp. 1–4.
28. Jia, S.; Yu, J.; Wang, J.; Wang, W.; Wu, Q.; Huang, G.; Yang, E. A Novel Optoelectronic Oscillator Based on Wavelength Multiplexing. *IEEE Photonics Technol. Lett.* **2015**, *27*, 213–216. <https://doi.org/10.1109/LPT.2014.2365231>.
29. Li, X.; Zhu, D.; Ding, J.; Hu, X.; Pan, S. Simulation investigation of coupled optoelectronic oscillator with high supermode suppression ratio. In Proceedings of the Seventh Asia Pacific Conference on Optics Manufacture and 2021 International Forum of Young Scientists on Advanced Optical Manufacturing (APCOM and YSAOM 2021), Shanghai, China, 28–31 October 2022; Volume 12166, pp. 1829–1834.
30. Zeng, H.; Yan, J. GHz repetition rate tunable optical pulses generation using a SBS-based coupled optoelectronic oscillator. *Opt. Commun.* **2024**, *555*, 130234. <https://doi.org/10.1016/j.optcom.2023.130234>.
31. Liu, Y.; Hao, T.; Li, W.; Capmany, J.; Zhu, N.; Li, M. Observation of parity-time symmetry in microwave photonics. *Light Sci. Appl.* **2018**, *7*, 38. <https://doi.org/10.1038/s41377-018-0035-8>.
32. Zhang, J.; Yao, J. Parity-time-symmetric optoelectronic oscillator. *Sci. Adv.* **2018**, *4*, eaar6782. <https://doi.org/10.1126/sciadv.aar6782>.
33. Zhang, F.; Lin, X.; Wu, Z.; Xia, G. A Symmetric Parity-Time Coupled Optoelectronic Oscillator Using a Polarization-Dependent Spatial Structure. *Photonics* **2023**, *10*, 1236. <https://doi.org/10.3390/photonics10111236>.
34. Fu, J.; Dai, Z.; Han, X.; Yao, J. Wavelength-Space Parity-Time Symmetric Optoelectronic Oscillator Using a Chirped Fiber Bragg Grating. *IEEE Photonics Technol. Lett.* **2024**, *36*, 187–190. <https://doi.org/10.1109/LPT.2023.3344683>.
35. Lelièvre, O.; Crozatier, V.; Berger, P.; Baili, G.; Llopis, O.; Dolfi, D.; Nouchi, P.; Goldfarb, F.; Bretenaker, F.; Morvan, L. A model for designing ultralow noise single-and dual-loop 10-GHz optoelectronic oscillators. *J. Light. Technol.* **2017**, *35*, 4366–4374.
36. Chen, J.; Zheng, Y.; Xue, C.; Zhang, C.; Chen, Y. Filtering effect of SiO₂ optical waveguide ring resonator applied to optoelectronic oscillator. *Opt. Express* **2018**, *26*, 12638–12647.
37. Yu, Y.; Tang, H.; Liu, W.; Hu, X.; Zhang, Y.; Xiao, X.; Yu, Y.; Zhang, X. Frequency stabilization of the tunable optoelectronic oscillator based on an ultra-high-Q microring resonator. *IEEE J. Sel. Top. Quantum Electron.* **2019**, *26*, 1–9.
38. Zhang, J.; Wang, Y.; Ding, Q. Single-loop tunable PT-symmetric optoelectronic oscillator based on a phase modulator. *Appl. Opt.* **2024**, *63*, 566–574.
39. Kaba, M.; Li, H.-W.; Daryoush, A.S.; Vilcot, J.-P.; Decoster, D.; Chazelas, J.; Bouwmans, G.; Quiquempois, Y.; Deborgies, F. Improving thermal stability of opto-electronic oscillators. *IEEE Microw. Mag.* **2006**, *7*, 38–47.
40. Zhang, L.; Poddar, A.K.; Rohde, U.L.; Daryoush, A.S. Comparison of optical self-phase locked loop techniques for frequency stabilization of oscillators. *IEEE Photonics J.* **2014**, *6*, 1–15.
41. Wang, Y.; Yan, J. Stability improvement of a dual-loop optoelectronic oscillator based on self-phase locking. *Appl. Opt.* **2022**, *61*, 8912–8916.
42. Jiang, Y.; Bai, G.; Hu, L.; Li, H.; Zhou, Z.; Xu, J.; Wang, S. Frequency locked single-mode optoelectronic oscillator by using low frequency RF signal injection. *IEEE Photonics Technol. Lett.* **2013**, *25*, 382–384.
43. Zhou, W.; Blasche, G. Injection-locked dual opto-electronic oscillator with ultra-low phase noise and ultra-low spurious level. *IEEE Trans. Microw. Theory Tech.* **2005**, *53*, 929–933.
44. Williams, C.; Quinlan, F.; Davila-Rodriguez, J.; Delfyett, P.J. Optical injection locking of a coupled optoelectronic oscillator. In Proceedings of the Conference on Lasers and Electro-Optics, Baltimore, MD, USA, 2–4 June 2009; Optica Publishing Group: Washington, DC, USA, 2009; p. CThF3. Available online: <https://opg.optica.org/abstract.cfm?uri=CLEO-2009-CThF3> (accessed on 17 November 2024).
45. Guan, S.; Cen, Q.; Yin, F.; Xu, K.; Dai, Y. Self-injection-locked optoelectronic oscillator based on frequency conversion filtering. *J. Light. Technol.* **2021**, *40*, 1888–1894.
46. Zhenghua, Z.; Chun, Y.; Zhewei, C.; Yuhua, C.; Xianghua, L. An ultra-low phase noise and highly stable optoelectronic oscillator utilizing IL-PLL. *IEEE Photonics Technol. Lett.* **2015**, *28*, 516–519.

47. Fu, R.; Jin, X.; Zhu, Y.; Jin, X.; Yu, X.; Zheng, S.; Chi, H.; Zhang, X. Frequency stability optimization of an OEO using phase-locked-loop and self-injection-locking. *Opt. Commun.* **2017**, *386*, 27–30.
48. Liu, Y.; Choudhary, A.; Marpaung, D.; Eggleton, B.J. Integrated microwave photonic filters. *Adv. Opt. Photonics* **2020**, *12*, 485–555. <https://doi.org/10.1364/AOP.378686>.
49. Liu, Q.; Fok, M.P. Adaptive photonic RF spectral shaper. *Opt. Express* **2020**, *28*, 24789–24798.
50. Eliyahu, D.; Maleki, L. Tunable, ultra-low phase noise YIG based opto-electronic oscillator. In Proceedings of the IEEE MTT-S International Microwave Symposium Digest, Philadelphia, PA, USA, 8–13 June 2003; Volume 3, pp. 2185–2187 vol.3.
51. Qi, H.; Lu, D.; Zhao, L. A Frequency-Tunable Coupled Optoelectronic Oscillator. In Proceedings of the 2021 Asia Communications and Photonics Conference (ACP), Shanghai, China, 24–27 October 2021; pp. 1–3. Available online: <https://ieeexplore.ieee.org/abstract/document/9738407> (accessed on 17 November 2024).
52. Peng, H.; Xie, X.; Zhang, C.; Sun, T.; Guo, P.; Chen, F.; Zhu, L.; Hu, W.; Chen, Z. Widely Tunable Dual Loop Optoelectronic Oscillator based on a Single-Bandpass Microwave Photonic Filter and a Recirculating Delay Line. In Proceedings of the 2014 Asia Communications and Photonics Conference (ACP), Shanghai, China, 11–14 November 2014; pp. 1–3. Available online: <https://ieeexplore.ieee.org/abstract/document/8687583> (accessed on 17 November 2024).
53. Wang, A.; Wo, J.; Zhang, J.; Luo, X.; Xu, X.; Zhang, D.; Du, P.; Yu, L. Radio-frequency arbitrary waveform generation based on dispersion compensated tunable optoelectronic oscillator with ultra-wide tunability. *Chin. Opt. Lett.* **2017**, *15*, 100603.
54. Li, C.; Wang, Y.; Wang, W.; Xu, Z.; Zhao, B.; Wang, H.; Tang, D. Widely Tunable Optoelectronic Oscillator Using a Dispersion-Induced Single Bandpass MPF. *IEEE Photonics Technol. Lett.* **2018**, *30*, 7–10. <https://doi.org/10.1109/LPT.2017.2765743>.
55. Li, W.; Yao, J. A Wideband Frequency Tunable Optoelectronic Oscillator Incorporating a Tunable Microwave Photonic Filter Based on Phase-Modulation to Intensity-Modulation Conversion Using a Phase-Shifted Fiber Bragg Grating. *IEEE Trans. Microw. Theory Tech.* **2012**, *60*, 1735–1742. <https://doi.org/10.1109/TMTT.2012.2189231>.
56. Yang, B.; Jin, X.; Zhang, X.; Zheng, S.; Chi, H.; Wang, Y. A wideband frequency-tunable optoelectronic oscillator based on a narrowband phase-shifted FBG and wavelength tuning of laser. *IEEE Photonics Technol. Lett.* **2011**, *24*, 73–75.
57. Dai, Z.; Fan, Z.; Li, P.; Yao, J. Frequency-tunable parity-time-symmetric optoelectronic oscillator using a polarization-dependent Sagnac loop. *J. Light. Technol.* **2020**, *38*, 5327–5332.
58. Shi, M.; Yi, L.; Hu, W. SBS-based OEO with high tuning resolution and wide tuning range by selecting different-order phase modulation sideband as pump. In Proceedings of the Optical Fiber Communication Conference, San Diego, CA, USA, 11–15 March 2018; Optica Publishing Group: Washington, DC, USA, 2018; p. M1H-4. Available online: <https://opg.optica.org/abstract.cfm?uri=OFC-2018-M1H.4> (accessed on 17 November 2024).
59. Peng, H.; Zhang, C.; Xie, X.; Sun, T.; Guo, P.; Zhu, X.; Zhu, L.; Hu, W.; Chen, Z. Tunable DC-60 GHz RF generation utilizing a dual-loop optoelectronic oscillator based on stimulated Brillouin scattering. *J. Light. Technol.* **2015**, *33*, 2707–2715.
60. Wu, Z.; Zhang, J.; Wang, Y. A Frequency Stable and Tunable Optoelectronic Oscillator Using an Optical Phase Shifter and a Phase-shifted Fiber Bragg Grating. *Curr. Opt. Photonics* **2022**, *6*, 634–641.
61. Ding, Q.; Wang, M.; Zhang, J.; Mu, H.; Wang, C.; Fan, G. A precisely frequency-tunable parity-time-symmetric optoelectronic oscillator. *J. Light. Technol.* **2020**, *38*, 6569–6577.
62. Zhou, P.; Zhang, F.; Pan, S. A multi-frequency optoelectronic oscillator based on a single phase-modulator. In Proceedings of the CLEO: Applications and Technology, San Jose, CA, USA, 8–13 June 2015; Optica Publishing Group: Washington, DC, USA, 2015; p. JTh2A-39. Available online: https://opg.optica.org/abstract.cfm?uri=cleo_at-2015-JTh2A.39 (accessed on 17 November 2024).
63. Yin, B.; Wang, M.; Wu, S.; Tang, Y.; Feng, S.; Zhang, H. High sensitivity axial strain and temperature sensor based on dual-frequency optoelectronic oscillator using PMFBG Fabry-Perot filter. *Opt. Express* **2017**, *25*, 14106–14113.
64. Wu, B.; Wang, M.; Dong, Y.; Tang, Y.; Mu, H.; Li, H.; Yin, B.; Yan, F.; Han, Z. Magnetic field sensor based on a dual-frequency optoelectronic oscillator using cascaded magnetostrictive alloy-fiber Bragg grating-Fabry Perot and fiber Bragg grating-Fabry Perot filters. *Opt. Express* **2018**, *26*, 27628–27638.
65. Zhou, P.; Zhang, F.; Pan, S. A tunable multi-frequency optoelectronic oscillator based on stimulated Brillouin scattering. In Proceedings of the 2015 14th International Conference on Optical Communications and Networks (ICOON), Nanjing, China, 3–5 July 2015; pp. 1–3. Available online: <https://ieeexplore.ieee.org/abstract/document/7203635/> (accessed on 17 November 2024).
66. Zhang, J.; Wang, Y.; Li, X.; Liu, Z.; Wo, J. Tunable multi-frequency optoelectronic oscillator based on a microwave photonic filter and an electrical filter. *Opt. Quantum Electron.* **2021**, *53*, 407. <https://doi.org/10.1007/s11082-021-03061-0>.

67. Fu, Z.; Zeng, Z.; Tian, H.; Lyu, W.; Zhang, Z.; Zhang, S.; Zhang, Y.; Li, H.; Liu, Y. Wide-Range Tunable Coherent Dual-frequency Microwave Signal Generation with Low Spurious Components in Optoelectronic Oscillator. *J. Light. Technol.* **2024**, *42*, 7443–7450. Available online: <https://ieeexplore.ieee.org/abstract/document/10551635/> (accessed on 16 January 2025).
68. Ge, Z.; Hao, T.; Capmany, J.; Li, W.; Zhu, N.; Li, M. Broadband random optoelectronic oscillator. *Nat. Commun.* **2020**, *11*, 5724. <https://doi.org/10.1038/s41467-020-19596-x>.
69. Hao, T.; Tang, J.; Li, W.; Zhu, N.; Li, M. Harmonically Fourier domain mode-locked optoelectronic oscillator. *IEEE Photonics Technol. Lett.* **2019**, *31*, 427–430.
70. Hao, T.; Tang, J.; Shi, N.; Li, W.; Zhu, N.; Li, M. Dual-chirp Fourier domain mode-locked optoelectronic oscillator. *Opt. Lett.* **2019**, *44*, 1912–1915.
71. Hao, P.; Dong, Z.; Han, D.; Huang, C.; Yao, X.S. Simultaneous dual-band frequency-agile microwave signal generation with a dual loop Fourier domain mode locked optoelectronic oscillator. *J. Light. Technol.* **2024**, *42*, 7710–7716. Available online: <https://ieeexplore.ieee.org/abstract/document/10475433/> (accessed on 16 January 2025).
72. Zhu, S.; Fan, X.J.; Xu, B.R.; Sun, W.H.; Li, M.; Zhu, N.H.; Li, W. Polarization manipulated Fourier domain mode-locked optoelectronic oscillator. *J. Light. Technol.* **2020**, *38*, 5270–5277.
73. Hao, T.; Tang, J.; Li, W.; Zhu, N.; Li, M. Tunable Fourier domain mode-locked optoelectronic oscillator using stimulated Brillouin scattering. *IEEE Photonics Technol. Lett.* **2018**, *30*, 1842–1845.
74. Hao, T.; Cen, Q.; Dai, Y.; Tang, J.; Li, W.; Yao, J.; Zhu, N.; Li, M. Breaking the limitation of mode building time in an optoelectronic oscillator. *Nat. Commun.* **2018**, *9*, 1839. <https://doi.org/10.1038/s41467-018-04240-6>.
75. Zhao, X.; Wu, B.; Wang, M.; Xiao, S.; Li, J.; Cai, Y.; Yan, F. Enhanced sensitivity of magnetic field sensing using L-shaped dual Terfenol-D-FBGs based on the Vernier effect and a dual-loop optoelectronic oscillator. *Opt. Express* **2024**, *32*, 29988–30002.
76. Feng, D.; Liu, Y.; Wang, H.; Deng, M. Faraday Rotation Angle Measurement Based on Coupled Optoelectronic Oscillator with Temperature Compensation. *J. Light. Technol.* **2024**, *42*, 8137–8143. Available online: <https://ieeexplore.ieee.org/abstract/document/10608388/> (accessed on 16 January 2025).
77. Xue, Z.; Li, S.; Li, J.; Xue, X.; Zheng, X.; Zhou, B. OFDM radar and communication joint system using opto-electronic oscillator with phase noise degradation analysis and mitigation. *J. Light. Technol.* **2022**, *40*, 4101–4109.
78. Li, P.; Shao, K.; Zhang, Y.; Pan, S. Optical pulse repetition rate division using an optoelectronic oscillator. *Chin. Opt. Lett.* **2024**, *22*, 043902.
79. Ma, Y.; Linghu, S.; Chen, B.; Gu, F. Continuous ultra-wideband signal regeneration in random optoelectronic oscillators through injection locking. *Opt. Express* **2024**, *32*, 9847–9856.
80. Xu, Z.; Tian, H.; Zhang, L.; Zhao, Q.; Zhang, Z.; Zhang, S.; Li, H.; Liu, Y. High-resolution radar ranging based on the ultra-wideband chaotic optoelectronic oscillator. *Opt. Express* **2023**, *31*, 22594–22602.
81. Dai, H.; Chembo, Y.K. RF fingerprinting based on reservoir computing using narrowband optoelectronic oscillators. *J. Light. Technol.* **2022**, *40*, 7060–7071.
82. Klimko, B.H.; Dai, H.; Chembo, Y.K. Resource-constrained narrowband optoelectronic oscillator-based reservoir computing for classification of modulated signals. *Opt. Lett.* **2024**, *49*, 3608–3611.
83. Ilgaz, M.A.; Batagelj, B. Opto-electronic oscillators for micro-and millimeter wave signal generation. *Electronics* **2021**, *10*, 857.
84. Zhang, W.; Yao, J. A silicon photonic integrated frequency-tunable optoelectronic oscillator. In Proceedings of the 2017 International Topical Meeting on Microwave Photonics (MWP), Beijing, China, 23–26 October 2017; pp. 1–4. Available online: <https://ieeexplore.ieee.org/abstract/document/8168643/> (accessed on 17 November 2024).
85. Pan, B.; Lu, D.; Zhang, L.; Zhao, L. A widely tunable optoelectronic oscillator based on directly modulated dual-mode laser. *IEEE Photonics J.* **2015**, *7*, 1–7.
86. Liu, P.; Xie, Z.; Lin, D.; Lu, M.; Cheng, W.; Hu, G.; Yun, B.; Cui, Y. Parity-time symmetric tunable OEO based on dual-wave-length and cascaded PS-FBGs in a single-loop. *Opt. Express* **2021**, *29*, 35377–35386.
87. Ahmadfard, F.; Hosseini, S.E. Design and simulation of a tunable parity-time symmetric optoelectronic oscillator utilizing integrated components. *Sci. Rep.* **2024**, *14*, 16014.
88. Tian, Y.; Han, Z.; Wang, L.; Zheng, Y.; Zhang, P.; Jiang, Y.; Xiao, H.; Zhou, X.; Yuan, M.; Low, M.X. Integrated Ultra-Wideband Tunable Fourier Domain Mode-Locked Optoelectronic Oscillator. 2024. Available online: <https://www.researchsquare.com/article/rs-4743222/latest> (accessed on 17 November 2024).
89. Dziallas, G.; Fatemi, A.; Peczek, A.; Tarar, M.; Kissinger, D.; Zimmermann, L.; Malignaggi, A.; Kahmen, G. A -115 dBc/Hz Integrated Optoelectronic Oscillator in a BiCMOS Silicon Photonic Technology. In Proceedings of the 2021 IEEE MTT-S

- International Microwave Symposium (IMS), Atlanta, GA, USA, 7–25 June 2021; pp. 23–26. Available online: <https://ieeexplore.ieee.org/abstract/document/9574906/> (accessed on 17 November 2024).
90. Li, J.; Pu, T.; Zheng, J.; Zhang, Y.; Shi, Y.; Shao, W.; Zhang, X.; Meng, X.; Liu, J.; Liu, J. All-optical gain optoelectronic oscillator based on a dual-frequency integrated semiconductor laser: Potential to break the bandwidth limitation in the traditional OEO configuration. *Opt. Express* **2021**, *29*, 1064–1075.
 91. Do, P.T.; Alonso-Ramos, C.; Le Roux, X.; Ledoux, I.; Journet, B.; Cassan, E. Wideband tunable microwave signal generation in a silicon-micro-ring-based optoelectronic oscillator. *Sci. Rep.* **2020**, *10*, 6982. <https://doi.org/10.1038/s41598-020-63414-9>.
 92. Hong, X.; Cheng, Y.; Wang, B.; Zhang, W. On-Chip photonic generation of tunable wideband phase-coded linearly-chirped microwave waveforms. *J. Light. Technol.* **2023**, *41*, 6199–6207.
 93. Hong, X.; Yu, Z.; Yu, W.; Wang, B.; Zhang, W. Independently Tunable Dual-Band Linearly-Chirped Microwave Waveforms Generation on a Silicon Photonic Chip. *J. Light. Technol.* **2024**, *42*, 5476–5484. Available online: <https://ieeexplore.ieee.org/abstract/document/10517378/> (accessed on 12 January 2025).
 94. Ivanov, V.; Voronkov, G.; Golubchikov, A.; Kuznetsov, I.; Grakhova, E.; Kutluyarov, R. PIC-based opto-electronic oscillator for communication and sensing applications. *J. Opt. Technol.* **2023**, *90*, 719–724.
 95. Wang, L.; Xiao, X.; Xu, L.; Liu, Y.; Chen, Y.; Yu, Y.; Zhang, X. On-chip tunable parity-time symmetric optoelectronic oscillator. *Adv. Photonics Nexus* **2023**, *2*, 016004.
 96. Zhang, G.; Hao, T.; Cen, Q.; Li, M.; Shi, N.; Li, W.; Xiao, X.; Qi, N.; Dong, J.; Dai, Y. Hybrid-integrated wideband tunable optoelectronic oscillator. *Opt. Express* **2023**, *31*, 16929–16938.
 97. Chen, G.; Lu, D.; Guo, L.; Deng, Q.; Zhao, W.; Zhao, L. An Optoelectronic Oscillator based on Self-Injection-Locked Monolithic Integrated Dual-mode Amplified Feedback Laser. In Proceedings of the Asia Communications and Photonics Conference, Guangzhou, China, 10–13 November 2017; Optica Publishing Group: Washington, DC, USA, 2017; p. Su2A.10.
 98. Li, P.; Dai, Z.; Fan, Z.; Yan, L.; Yao, J. Parity-time-symmetric frequency-tunable optoelectronic oscillator with a single dual-polarization optical loop. *Opt. Lett.* **2020**, *45*, 3139–3142. <https://doi.org/10.1364/OL.394719>.
 99. Ma, R.; Huang, Z.; Gao, S.; Wang, J.; Wang, X.; Zhang, X.; Hao, P.; Yao, X.S.; Cai, X. Ka-band thin film lithium niobate photonic integrated optoelectronic oscillator. *Photonics Res.* **2024**, *12*, 1283–1293.
 100. Han, J.-Y.; Huang, Y.-T.; Hao, Y.-Z.; Tang, M.; Wang, F.-L.; Xiao, J.-L.; Yang, Y.-D.; Huang, Y.-Z. Wideband frequency-tunable optoelectronic oscillator with a directly modulated AlGaInAs/InP integrated twin-square microlaser. *Opt. Express* **2018**, *26*, 31784–31793. <https://doi.org/10.1364/OE.26.031784>.
 101. Zhang, X.; Zheng, J.; Pu, T.; Zhang, Y.; Shi, Y.; Li, J.; Li, Y.; Zhu, H.; Chen, X. Simple frequency-tunable optoelectronic oscillator using integrated multi-section distributed feedback semiconductor laser. *Opt. Express* **2019**, *27*, 7036–7046. <https://doi.org/10.1364/OE.27.007036>.
 102. Teng, C.; Zou, X.; Li, P.; Pan, W.; Yan, L. Wideband Frequency-Tunable Parity-Time Symmetric Optoelectronic Oscillator Based on Hybrid Phase and Intensity Modulations. *J. Light. Technol.* **2020**, *38*, 5406–5411.
 103. Fan, Z.; Zhang, W.; Qiu, Q.; Yao, J. Hybrid Frequency-Tunable Parity-Time Symmetric Optoelectronic Oscillator. *J. Light. Technol.* **2020**, *38*, 2127–2133.
 104. Liu, P.; Zheng, P.; Yang, H.; Lin, D.; Hu, G.; Yun, B.; Cui, Y. Parity-time symmetric frequency-tunable optoelectronic oscillator based on a Si₃N₄ microdisk resonator. *Appl. Opt.* **2021**, *60*, 1930–1936. <https://doi.org/10.1364/AO.417003>.
 105. Zou, F.; Zou, L.; Lai, Y.; Xie, C.; Luo, J.; Milosevic, D.; Yan, L.; Pan, W.; Liu, Y.; Cao, Z.; et al. Parity-Time Symmetric Optoelectronic Oscillator Based on an Integrated Mode-Locked Laser. *IEEE J. Quantum Electron.* **2021**, *57*, 1–9. <https://doi.org/10.1109/JQE.2021.3051410>.
 106. Wang, L.; Liu, Y.; Chen, Y.; Gou, W.; Cui, S.; Yu, Y.; Xiao, X.; Yu, Y.; Zhang, X. Generation of Reconfigurable Linearly Chirped Microwave Waveforms Based On Fourier domain Mode-Locked Optoelectronic Oscillator. *J. Light. Technol.* **2022**, *40*, 85–92.
 107. Gou, W.; Wang, L.; Liu, Y.; Chen, Y.; Yu, Y.; Yu, Y.; Zhang, X. Generation of Phase-Coded LFM Signals Based on Fourier Domain Mode-Locked Optoelectronic Oscillator. *J. Light. Technol.* **2023**, *41*, 6142–6148. <https://doi.org/10.1109/JLT.2023.3282992>.

Disclaimer/Publisher’s Note: The statements, opinions and data contained in all publications are solely those of the individual author(s) and contributor(s) and not of MDPI and/or the editor(s). MDPI and/or the editor(s) disclaim responsibility for any injury to people or property resulting from any ideas, methods, instructions or products referred to in the content.